

Data-driven generalized perimeter control: Zürich case study

Alessio Rimoldi * ¹, Carlo Cenedese^{1,2}, Alberto Padoan³, Florian Dörfler¹, and John Lygeros¹

¹Automatic Control Laboratory, ETH Zürich ([arimoldi](mailto:arimoldi@ethz.ch), [jlygeros](mailto:jlygeros@ethz.ch), fdorfler@ethz.ch)

²Delft Center for Systems and Control, TU Delft (ccenedese@tudelft.nl)

³Dep. of Electrical and Computer Engineering, UBC (alberto.padoan@ubc.ca)

February 28, 2026

Abstract

Urban traffic congestion is a key challenge for the development of modern cities, requiring advanced control techniques to optimize existing infrastructures usage. Despite the extensive availability of data, modeling such complex systems remains an expensive and time consuming step when designing model-based control approaches. On the other hand, machine learning approaches require simulations to bootstrap models, or are unable to deal with the sparse nature of traffic data and enforce hard constraints. We propose a novel formulation of traffic dynamics based on behavioral systems theory and apply data-enabled predictive control to steer traffic dynamics via dynamic traffic light control. A high-fidelity simulation of the city of Zürich, the largest closed-loop microscopic simulation of urban traffic in the literature to the best of our knowledge, is used to validate the performance of the proposed method in terms of total travel time and CO₂ emissions.

1 Introduction

As cities worldwide grow at an ever-increasing pace, infrastructures struggle under the stress of increasing demand. The United Nations forecasts that by 2050, 68% of the total world population will live in urban centers [1]. Roads remain by far the preferred mode of transport for people and goods both in the United States and the European Union [2], accounting for 74% of land freight transport in the European Union during 2021 [3]. The combination of these factors will make the problem of reducing urban traffic congestion even more challenging. Estimates show that road transport generates 12% of human CO₂ emissions and urban air pollution has been linked to a host of negative health effects [4]. Traffic congestion also leads to economic loss, due to unrealized productivity, valued between 1-2% of the European Union total gross domestic product (80 to 160 billion euros per year) [5]. Infrastructural changes aimed at solving this problem are limited in scale by prohibitive cost and their effects are difficult to predict due to counterintuitive phenomena such as the Braess paradox [6]. For this reason optimization of existing infrastructure through traffic management systems is often a preferable solution.

Adaptive traffic signal control is the most widespread form of urban traffic management [7], due to its effectiveness and relative low cost. The most common approach is to derive a model of the city's traffic dynamics and then apply model-based control algorithms such as Model Predictive Control (MPC) to compute optimal inputs for the traffic lights [8]. This methodology was proven to be effective [8, 9] and easily integrates prior knowledge about the system into the model. However, modeling such large systems is expensive and

*This work was supported as a part of NCCR Automation, a National Center of Competence in Research, funded by the Swiss National Science Foundation (grant number 51NF40_225155)

A. Padoan acknowledges the support of the Natural Sciences and Engineering Research Council of Canada (NSERC). Grant numbers: RGPIN-2025-06895 and DGECR-2025-00382

time consuming due to the dynamic large-scale nature of a city, where the road network is often subject to changes (e.g., road closures) and demand changes over time. The availability of data is an opportunity to approach the problem differently. Thanks to data-informed decision-making algorithms, it is now possible to identify and exploit complex patterns to efficiently control traffic. Data-driven methods are some of the most promising approaches when dealing with large-scale systems as they have been shown to produce robust control policies without requiring explicit modeling [10–12]. Current research in this area focuses on machine learning techniques, such as deep reinforcement learning, which have been proven to be effective when controlling traffic systems [11, 13]. Training models directly on traffic data can nonetheless be challenging due to its sparse nature and the effects of an input being delayed in time. Deep reinforcement learning is known to require large datasets to produce satisfactory policies. Synthetic data produced by simulations can be used, but this requires a model to simulate in the first place.

Recently, Data-enabled Predictive Control (DeePC) has been applied to the Intersection Traffic Signal Control Problem (ITSCP) showing promising results through Simulation-based Optimization (SimOpt) on a lattice network [10]. This method has the advantage of not needing an explicit model, as it bases its representation of the traffic dynamics directly on data collected from the system, requiring less parameters and retaining higher interpretability compared to machine learning procedures.

Even though the ITSCP has been a subject of research for over 70 years, there still exists a gap between the literature and practical implementations [7]. One of the main reasons behind this gap is the lack of a common benchmark in the field. Most of the traffic research so far has focused on several different small networks due to computational cost (see Section 1.1.6). These networks are often too simple to allow conclusions to be drawn about real urban traffic networks and their differences make comparing different approaches difficult. With this in mind, this work builds on previous results [10], showing that solving the ITSCP via DeePC is a general approach able to handle large-scale networks and generic intersections. We corroborate our findings through closed-loop microscopic simulations based on the Simulation of Urban MObility (SUMO) package, using a real-scale high-fidelity simulation of the city of Zürich.

1.1 Literature Review

The ITSCP is a complex problem involving many factors, such as human behavior, vehicle interactions within the network, stochastic traffic demand, and unpredictable events (e.g. traffic accidents). For these reasons, it has been the subject of extensive research since the seminal work in [14] and the development of TRAFFIC Network Study Tool (TRANSYT) [15]. In this section, we give a brief overview of the relevant literature on traffic signal control, for a more in-depth overview we refer the interested reader to [7, 16, 17].

1.1.1 Rule-Based

Many early approaches employed rule-based methods to solve the ITSCP. Rule-based methods work by defining states and a set of appropriate actions associated with each state to optimize a performance criterion. An example of these early methods can be found in [18–20], where the authors developed the saturation flow algorithm. In [21] a rule-based algorithm is combined with fuzzy logic. Fuzzy rule-based systems derive actions from given inputs by defining if-then rules which represent the relationship between the variables [22–25]. In [26] the authors devise a dynamic rule-based system that changes the rules depending on traffic conditions to handle problems in real time. However, as noted by [27], it can be difficult to generate effective rules, especially for general intersections with a large number of possible phases.

1.1.2 Dynamic Programming

Dynamic programming has been applied to the ITSCP to develop flexible control algorithms applicable to a variety of traffic conditions. The authors of [28] first applied dynamic programming using phases and stages as control variables. In [29] an algorithm based on dynamic programming capable of controlling an arterial network was developed. In [30] was shown that an adaptive traffic signal controller using approximate dynamic programming and reinforcement learning is capable of reducing vehicle delays. In [31], the authors

developed a recursive data pipeline comprising data processing, flow prediction, parameter optimization, and signal control. The main drawback of these methods is their computational complexity, which makes scaling to large scale urban traffic networks difficult. Complexity can be mitigated by using techniques such as approximate dynamic programming at the expense of performance.

1.1.3 Distributed and Multi-Agent Methods

Recently, there has been multiple attempts to control traffic networks in a distributed way [11–13, 32–36]. A popular distributed algorithm in traffic light control is Max-pressure, derived from the backpressure scheduling framework [37]. The algorithm maximizes network throughput by selecting, at each intersection, the phase with the largest upstream-downstream queue differential. The authors of [36] proved that a fully distributed implementation of Max-pressure stabilizes any feasible demand distribution without requiring forecasts. In [35] the store-and-forward model is derived and the authors show that Max-pressure control is able to maximize the stability region using only local measurements and turn ratios. A practical drawback of classical Max-pressure theory is that it may induce highly variable cycle lengths and rapid phase switching, moreover, it does not incentivize coordination across the network. Multi-agent learning and game-theoretic approaches are also used in this context. The authors of [32] were able to deal with computational challenges by devising a distributed control approach and tested it on a simulated 9 by 7 grid network. The authors of [33] model an intersection as a non-cooperative game in which each player (traffic signal) aims at minimizing its queue and the solution of the ITSCP is the Nash equilibrium of the game. In [11–13, 34], the authors used reinforcement learning to implement cooperative hierarchical multi-agent systems for real-time signal timing control of complex traffic networks. A drawback of these methodologies is the inherent difficulty to provide theoretical guarantees such as stability or convergence. This is, however, a very active area of research.

1.1.4 Model Predictive Control

MPC is a powerful control methodology providing strong theoretical guarantees on the stability, feasibility, and optimality of the closed-loop system, under the assumption of having a model that well describes the real system [38]. An example of its application to the ITSCP can be found in [9], where a linear-parameter varying formulation of MPC for perimeter flow control is presented. This line of work is based on the partitioning of the network into regions described by the Macroscopic Fundamental Diagram (MFD) [39–41]. In [42], a similar approach is presented using economic MPC and regional route-guidance actuation-based control. The authors in [43] propose two different macroscopic models of urban traffic to design an MPC algorithm able to compute a structured network-wide traffic controller. These approaches are computationally efficient and allow for centralized control of large networks as shown in [9]. However, model estimation procedures for such large systems can be computationally demanding.

1.1.5 Data-enabled Predictive Control

Recently, there has been a surge of interest for data-driven control approaches [44]. In this regard, behavioral system theory [45] offers a powerful tool to obtain systems descriptions directly from data. The main idea is that the set of all possible trajectories of a dynamical system, called the *behavior*, contains all the information necessary to describe the system. Behaviors of linear systems can be represented by non-parametrized models. For linear systems, such representations are images of matrices containing data sampled from the system; these can then be leveraged by control algorithms. A particularly successful direct data-driven control algorithm obtained in this way is DeePC [46], which has been applied to numerous practical studies [46–48]. DeePC has been also applied to urban traffic control, in the contexts of connected and autonomous vehicles coordination [49] and vehicle rebalancing in mobility-on-demand systems [50]. We have previously shown DeePC to be effective in tackling the ITSCP on a symmetric lattice network comprising 64 intersections [10]. In this work we show that DeePC is suitable for controlling much larger networks with general intersection layouts.

1.1.6 Simulation-based Optimization

SimOpt is a field in which optimization techniques are integrated with simulation analysis [51]. Simulation tools are frequently used in ITSCP research, approximately 77% of the papers in the field use a simulation framework [17]. *AIMSUN* [52], *CORSIM* [53], *MATSim* [54], *Paramics* [55], SUMO [56], *VISSIM* [57]

are some of the most widely used simulation packages in research and industry. The majority of papers analyzed in [17] uses *VISSIM* as a simulation platform, closely followed by SUMO. Most works focus on isolated single intersections [58–62] and regular lattice networks [63–67]. Some papers consider controlled roundabouts [68, 69] and arterial networks [70, 71]. In recent years, more general networks have been the focus of attention; for example, the authors of [72] considered a part of the city of Changsha, China as a simulation setting. In [73–75], the traffic networks of Skopje, Northern Macedonia; Bologna, Italy; and Lausanne, Switzerland were simulated. The largest online closed-loop simulation, to the best of the authors knowledge is described in [9, 76] where a part of Barcelona, Spain is used as a network, serving 79,143 vehicles throughout the simulation. It is important to note that all these simulations make the unrealistic assumption that all intersections are four-legged intersections or do not regulate traffic flow at intersections; for example, [76] directly controls the flows between regions.

1.2 Contributions

The main contributions of this paper are three:

- (i) We introduce a flexible formulation of the ITSCP based on behavioral theory that can seamlessly incorporate different kinds of data and generalize classical perimeter control [8], the formulation accommodates other forms of actuation, such as dynamic speed limits,
- (ii) we conjecture a linear relationship between the traffic density and dynamic traffic light signals. We validate this conjecture using extensive high-fidelity simulations,
- (iii) we perform closed loop control on what is, to the best of our knowledge, the largest microsimulation in the literature equipped with demand estimated from real data. We propose the simulation as a standard benchmark in traffic control research and use it to validate the performance of the proposed methodology in terms of travel time and emissions metrics.

The paper is organized as follows. Section 2 describes the methodological framework, casting the ITSCP problem in the framework of behavioral system theory [77]. Section 3 presents the DeePC algorithm. Section 4 presents the simulation framework, the traffic networks used to test our method and numerical results showcasing the effectiveness of the closed-loop control. Section 5 summarizes our findings and future research directions.

Notation \mathbb{N} denotes the set of positive integer numbers, \mathbb{R} , \mathbb{R}^n and $\mathbb{R}^{p \times m}$ denote the set of real numbers, the set of n -dimensional vectors with real entries, and the set of $p \times m$ matrices with real entries, respectively. For every $p \in \mathbb{N}$, the set of positive integers $\{1, 2, \dots, p\}$ is denoted by \mathbf{p} . I denotes the identity matrix. A map f from X to Y is denoted by $f : X \rightarrow Y$; $(Y)^X$ denotes the collection of all such maps. The restriction of $f : X \rightarrow Y$ to a set X' such that $X' \cap X \neq \emptyset$ is denoted by $f|_{X'}$ and defined as $f|_{X'}(x) = f(x)$ for $x \in X \cap X'$. For $\mathcal{F} \subset (Y)^X$, then $\mathcal{F}|_{X'}$ denotes $\{f|_{X'} : f \in \mathcal{F}\}$.

2 Behavioral formulation of urban traffic dynamics

2.1 Traffic network, sensing and demand

We consider the traffic network of a city composed of intersections and roads, each divided into one or more lanes. Following [42], we partition a city in $p \in \mathbb{N}$ regions of homogeneous average traffic density to leverage the concept of MFD, see Figure 6. We use the MFD to obtain a reference trajectory for DeePC to track, as will be discussed in Section 2.3. Several methods can be used to generate such a partitioning [78], here we use a parallelized version of the *snake clustering* algorithm [79], detailed in Appendix B. The algorithm finds connected clusters of roads with homogeneous average traffic density, yielding a low-scatter MFD. The set of resulting regions is defined as $\mathbf{p} := \{1, \dots, p\}$.

The most common sensors used by municipalities to measure traffic conditions are *Eulerian* sensors [80], which are stationary devices, as opposed to *Lagrangian* [81] sensors which can be mobile. Throughout this

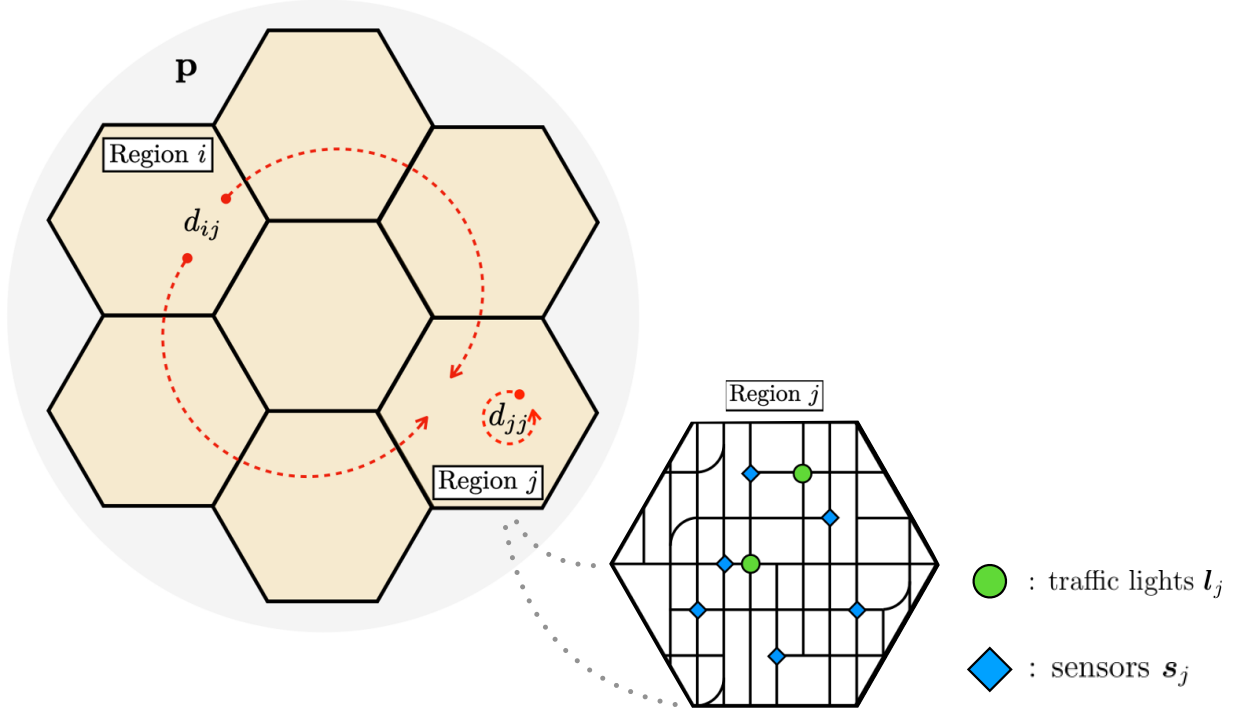


Figure 1: The city is divided into p regions homogeneous in average traffic density (the hexagons) and the demand \mathbf{d} among them. A detail of sensors \mathbf{s}_j (blue diamonds) and traffic lights \mathbf{l}_j (green circles) locations within region $j \in \mathbf{p}$ is shown.

paper, we assume the use of *Eulerian* sensors, capable of measuring traffic density and flow. However, proposed procedure is agnostic to the type of sensors used and Lagrangian sensors could be integrated [82]. We denote the set of sensors in region $i \in \mathbf{p}$ as $\mathbf{s}_i := \{1, \dots, s_i\}$, where $s_i \in \mathbb{N}$ is the number of sensors in the region. From each sensor $j \in \mathbf{s}_i$, we obtain the traffic density $\rho^j(t)$ [veh/km] and flow $\phi^j(t)$ [veh/h], at time $t \in \mathbb{T} \subseteq \mathbb{N}$, on the road where the sensor is located, normalized by the number of lanes. We then average the measurements over each region $i \in \mathbf{p}$, to reduce the variability and capture macroscopic variations [41]. We denote the average density and flow in region $i \in \mathbf{p}$ at time $t \in \mathbb{T}$ as

$$\rho_i(t) := \frac{1}{s_i} \sum_{j=1}^{s_i} \rho^j(t) \quad (1a)$$

$$\phi_i(t) := \frac{1}{s_i} \sum_{j=1}^{s_i} \phi^j(t) \quad (1b)$$

The vectors of average densities and flows in the city at time t are then,

$$\boldsymbol{\rho}(t) := [\rho_i(t)]_{i=1}^p \in \mathbb{R}^p \quad (2a)$$

$$\boldsymbol{\phi}(t) := [\phi_i(t)]_{i=1}^p \in \mathbb{R}^p \quad (2b)$$

The evolution of $\boldsymbol{\rho}$ and $\boldsymbol{\phi}$ depends on the flow of vehicles entering the traffic network during every time interval, known as the *demand*. The flow of vehicles starting their trip in region $i \in \mathbf{p}$ at time t with final destination in region $j \in \mathbf{p}$, is denoted by $d_{ij}(t)$ [veh/h]; $d_{ii}(t)$ is the internal demand of region i , as seen in Figure 1. The vector of demands starting in region i is denoted by $\mathbf{d}_i(t) := [d_{ij}(t)]_{j=1}^p \in \mathbb{R}^p$, while the

vector of all the demands among all regions is $\mathbf{d}(t) := [\mathbf{d}_i(t)]_{i=1}^p \in \mathbb{R}^{p^2}$. Despite being influenced by many factors such as commuters choices and weather conditions, $\mathbf{d}(t)$ presents seasonal patterns at different time scales, weekly, monthly, and yearly, that make it possible to reliably estimate it [83]. Demand estimation, in the form of time dependent origin-destination pairs, is a well-known problem and has been extensively studied [84, 85]. In this work, we do not consider the problem of predicting the demand and instead we consider it as a given exogenous input to the system.

2.2 Intersection Control

Following [7], we define an *intersection* as a set of *approaches* and a *crossing area*. The *crossing area* is the portion of space delimited by the stop lines of the approaches, where vehicles and pedestrians are allowed to cross intermittently under right of way. An *approach* is a road leading to the crossing area, comprising one or more *lanes*, each equipped with a *signal head*. Signal heads can be in one of three states: *green* (g), *yellow* (y), or *red* (r); the set of all the signal heads in the intersection makes up the *traffic signal* of the intersection. Approaches are used by *traffic flows* to reach the crossing area. Two flows are said to be *compatible* when the vehicles composing them can pass the crossing area simultaneously under right of way; otherwise they are called *antagonistic*. Figure 2 shows a simplified drawing of an intersection. On the left the crossing area, approach, lane and signal heads are highlighted for clarity. On the right the difference between compatible and antagonistic flows can be seen.

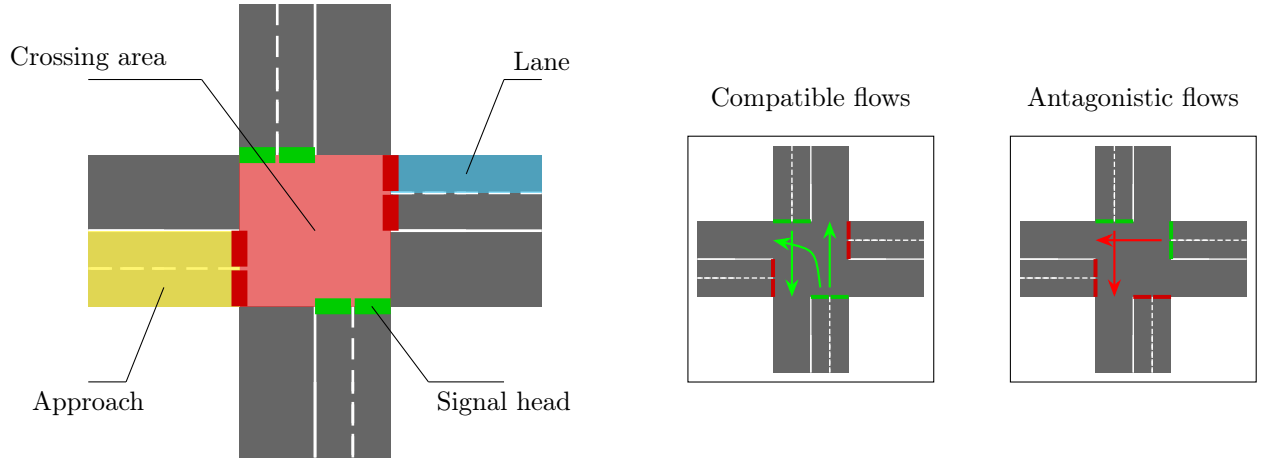


Figure 2: Example of a four-legged intersection and compatibility of traffic flows. On the left the structural components of the intersection are highlighted for clarity. On the right the difference between compatible and antagonistic flows can be observed.

A traffic signal *duty cycle*, is an ordered set Π of *phases*, its duration is called *cycle time* Δ_{dc} . A *phase* is a tuple containing the state value for each signal head, and is designed to allow compatible traffic flows to cross the intersection. Figure 3 illustrates a duty cycle for a four legged intersection, where a phase of only red states is used to clear the intersection.

By influencing the flow of vehicles traveling through an actuated intersection, it is possible to indirectly influence $\phi_i(t)$ and $\rho_i(t)$. Given two regions $i, j \in \mathbf{p}$, if one intersection sitting at the boundary between i and j can be actuated, one can regulate the flow of vehicles moving between the two regions at that point. If one can control all the access points from region i to j , then the flow of vehicles moving between the two regions can be directly controlled, that is, classical perimeter control [42]. Remarkably, our approach does not assume the actuators to be placed at the boundaries of the regions, as this is rarely the case in practice. Instead, we allow the actuators to be placed anywhere within the network, see Figure 1. According to [7], there are four possible approaches when controlling traffic light operations:

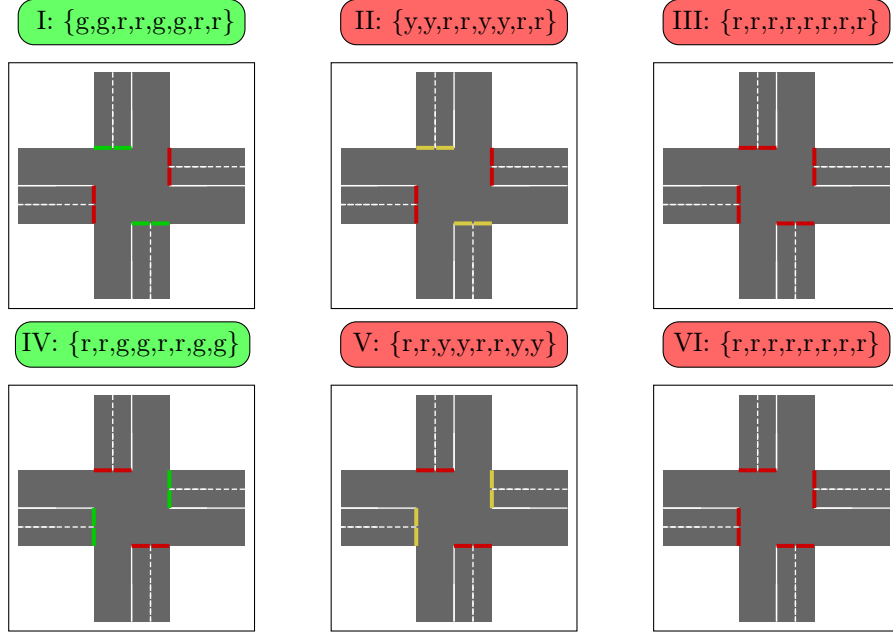


Figure 3: Example of a duty cycle comprising six phases divided in active and passive. Active phases (I,IV) are grouped in the leftmost column and highlighted in green, while passive phases (II,III,V,VI) can be found in the two rightmost columns highlighted in red. Active phases have at least one 'g' state in the tuple.

- *Phase specification*: The control input is the state composition of the phases. When dealing with complex intersections involving a multiple approaches, the specification of the optimal composition of the phases is non-trivial and has a major impact on the intersection's efficiency, often giving rise to mixed-integer problems [86].
- *Split control*: The control input is the duration of each phase as a portion of the duty cycle time Δ_{dc} . This duration can be optimized based on current network conditions.
- *Cycle time*: The control input is the cycle time Δ_{dc} . Longer cycle times lead to an increase in efficiency due to the smaller proportion that the constant lost times occupy, however, this may increase vehicle delays in underutilized intersections due to the longer red phase.
- *Offset*: The control input is the phase difference between the duty cycles of multiple successive intersections. In contrast to previous schemes, this approach assumes multiple intersections to be actuated. This can be used, for example, to generate a *green wave* along an arterial.

In this work, we focus on *split control* with fixed duty cycle time Δ_{dc} , making our method a fixed-time adaptive strategy in the classification of [7]. Under this scheme, the optimization problem can be readily formulated as a quadratic program with continuous bounded inputs. This problem can be solved efficiently, enabling practical implementations where the response time of the system is constrained.

We consider the *Split control* scheme with fixed duty cycle time Δ_{dc} for each controlled intersection. The actuated intersections are acting under the coordination of a centralized controller. The duty cycle of ℓ -th actuated intersection, is a finite ordered set Π_ℓ whose elements are referred to as *phases*. Given an intersection with n approaches each equipped with a signal head that can be red (r), yellow (y) or green (g) for any time interval, we define a *phase* as the n -tuple $y \in \{r, y, g\}^n$, where the i -th element represents the state of the i -th signal head. We associate to each phase $i \in \Pi_\ell$ a duration $\delta_i \in \mathbb{N}$ in seconds and we define the duty

cycle time $\Delta_{\text{dc}}^\ell \in \mathbb{N}$ as

$$\Delta_{\text{dc}}^\ell = \sum_{i \in \Pi_\ell} \delta_i.$$

When a phase contains at least one 'g' value we call it an *active phase*; otherwise, we call it a *passive phase*. Note that we include the duration of yellow phases in the duration of passive phases, see Figure 3. The set of active phases for the ℓ -th traffic light is denoted as $\mathcal{A}_\ell \subset \Pi_\ell$, the set of passive phases corresponds to \mathcal{A}_ℓ^c . Intuitively, the main difference between an active phase and a passive one is that during an active phase, some vehicles are allowed to cross the intersection. The duration of the *active* and *passive* phases are

$$\delta_a = \sum_{i \in \mathcal{A}_\ell} \delta_i, \quad \text{and} \quad \delta_p = \sum_{i \in \mathcal{A}_\ell^c} \delta_i = \Delta_{\text{dc}}^\ell - \delta_a,$$

respectively.

We define the percentage of time, with respect to the duty cycle time, for which an intersection is active as $\lambda_\ell = \delta_a / \Delta_{\text{dc}}^\ell \in [0, 1)$, $0 \leq \delta_a \leq \Delta_{\text{dc}}^\ell$. By controlling the value λ_ℓ one controls the fraction of Δ_{dc} for which the intersection is active, where a value $\lambda_\ell(t) = 0$ corresponds to an intersection with all the signal heads red for the whole duty cycle. Note that while the value $\lambda_\ell(t) = 0$ is achievable, the value $\lambda_\ell(t) = 1$ is not due to the constant duration of the yellow phases embedded in the passive phase duration. For the sake of simplicity, we consider the values $\lambda_\ell(t)$ to be real numbers, and we recover the corresponding δ_a by means of a floor operation. Figure 4 shows an example of input trajectory and for the ℓ -th traffic light and the resulting values of δ_a and δ_p .

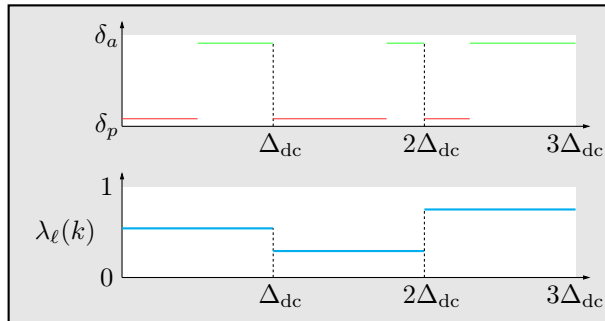


Figure 4: Different control input values λ_ℓ result in different active and passive phase durations, that is δ_a and δ_p , for a traffic light $\ell \in \mathbf{l}$. The bottom graph shows a possible input trajectory for the ℓ -th traffic light spanning three duty cycles, the top graph shows proportion of duty cycle time assigned to the active and passive phases as a result of the input.

We define the control input given to our system at time t as the vector $\boldsymbol{\lambda}(t) := [\lambda_i(t)]_{i=1}^l \in \mathbb{R}^l$, with $\mathbf{l} := \{1, \dots, l\}$ denoting all the actuated traffic lights. This formulation allows one to control a general intersection with a single scalar bounded input $\lambda_\ell(t)$. However, it comes with the disadvantage of relinquishing control over the durations of the individual phases, which determine traffic flows with different directionalities. To mitigate this shortcoming, one could introduce additional inputs to distinguish between different phases, at the cost of a more computationally expensive optimization problem. We assume that the traffic demand on one side of the intersection has greater magnitude than the opposite direction, which is often the case during peak hours. Under this assumption, the control input $\lambda_\ell(t)$ is sufficient to decongest the intersection.

2.3 Macroscopic fundamental diagram

The concept of MFD captures the relation between the flow ϕ_i and density ρ_i within a region $i \in \mathbf{p}$. For each region $i \in \mathbf{p}$ we plot the measurements of (ρ_i, ϕ_i) against each other and estimate the MFD using a 4-th degree polynomial, see Figure 6. We then use the estimated MFD to identify each region's critical density and maximal density, denoted as $\rho_{\text{cr},i}$, and $\rho_{\text{max},i}$, respectively. The critical density $\rho_{\text{cr},i}$ corresponds to the

abscissa of the maximum point for the MFD of region i , where the region reaches its maximum possible flow and throughput. This observation will be used later in Section 3 to define the reference trajectory to be tracked. We define the vector of critical densities as $\boldsymbol{\rho}_{\text{cr}} := [\rho_{\text{cr},i}]_{i=1}^p \in \mathbb{R}^p$. The maximal density $\rho_{\text{max},i}$ is the smallest positive root of the polynomial used to estimate the MFD, where the network reaches its maximum capacity and the flow equals zero. This state is often referred to as grid-lock, and we define the vector of the maximal densities as $\boldsymbol{\rho}_{\text{max}} := [\rho_{\text{max},i}]_{i=1}^p \in \mathbb{R}^p$.

The MFD captures the non-linear and non-injective relation that exists between the density ρ_i and flow ϕ_i in each region $i \in \mathbf{p}$. As we will discuss in Section 3, DeePC works best under an approximately linear relationship between the input and output measurements of the system. Despite the non-linear dependencies encoding the system dynamics through the MFD, as shown in Section 4 and supported by [10], the DeePC algorithm is able to find effective control policies using $\boldsymbol{\lambda}$ as the control input and $\boldsymbol{\rho}$ as the output measurement. This observation leads us to conjecture that the relationship between the input $\boldsymbol{\lambda}$ and the density $\boldsymbol{\rho}$ must be approximately linear. Moreover, empirical trials conducted by the authors using only the flow $\boldsymbol{\phi}$ or a combination of flow and density $\mathbf{y}(t) := \text{col}(\boldsymbol{\phi}(t), \boldsymbol{\rho}(t))$ as output of the system resulted in degraded performance of the algorithm (data not shown). This makes us conjecture that the relationship between $\boldsymbol{\lambda}$ and $\boldsymbol{\phi}$ must be non-linear, a fact that is not surprising given the non-linear relationship between density and flow. The two conjectures are summarised in the commutative diagram in Figure 5.

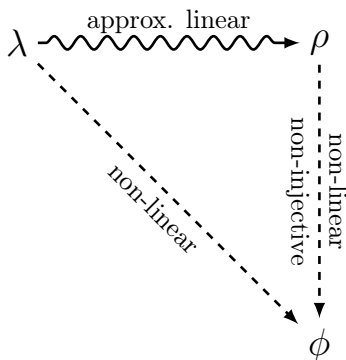


Figure 5: Commutative diagram of the relationships between λ , ρ and ϕ . The relationship between ρ and ϕ is assumed to be a MFD similar to Figure 6.

2.4 Behavioral traffic dynamics

We model traffic as a dynamical system using behavioral system theory [45, 87, 88]. The resulting formulation naturally generalizes perimeter traffic control by allowing the actuators to be placed anywhere in the network. A behavioral formulation is flexible, as it can in principle integrate any kind of measurement data. For example, in a traffic system, one could consider CO₂ emissions or noise as alternative outputs of the system. Below we give a brief introduction to behavioral systems theory, the interested reader is referred to Appendix A for more details.

In behavioral systems theory a *dynamical system* (or, briefly, *system*) is a triple $\Sigma = (\mathbb{T}, \mathbb{W}, \mathcal{B})$ [45], where \mathbb{T} is the *time set*, \mathbb{W} is the *signal set*, and $\mathcal{B} \subseteq (\mathbb{W})^{\mathbb{T}}$ is the *behavior* of the system. The behavior characterises the set of all signal trajectories over the time set \mathbb{T} that are compatible with the system. More specifically, if the signal set is $\mathbb{W} = \mathbb{R}^q$ the set of finite trajectories $w = (w(1), \dots, w(T))$ of length $T \in \mathbb{N}$, with $w(t) \in \mathbb{W}$ for $t \in \mathbb{T} := [1, \dots, T] \subset \mathbb{N}$, is $\mathbb{W}^{\mathbb{T}} = (\mathbb{R}^q)^{\mathbb{T}}$ and the behavior is a subset $\mathcal{B} \subseteq (\mathbb{R}^q)^{\mathbb{T}}$. We identify every finite trajectory $w \in (\mathbb{R}^q)^{\mathbb{T}}$ with the corresponding vector $\text{col}(w(1), \dots, w(T)) \in \mathbb{R}^{qT}$. In this case, a system Σ is called *linear* if the corresponding behavior \mathcal{B} is a linear subspace, and *time-invariant* if \mathcal{B} is shift-invariant, *i.e.*, if $w \in \mathcal{B}$ implies $\sigma w \in \mathcal{B}$, where σ is the *shift operator* defined as $(\sigma w)(t) := w(t + 1)$. The class of all complete Linear Time-Invariant (LTI) systems is denoted by \mathcal{L}^q , and for simplicity we write $\mathcal{B} \in \mathcal{L}^q$ to denote a linear behavior.

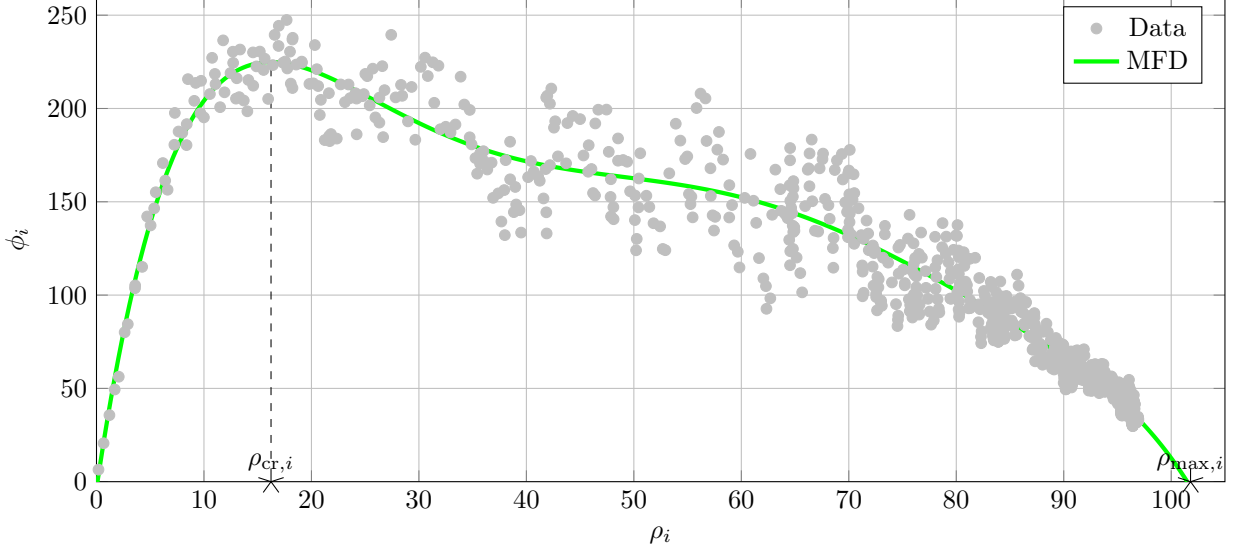


Figure 6: The MFD for the region of Wiedikon, Zürich (solid green line) simulated below. The critical density $\rho_{\text{cr},i}$ is the density where the flow is maximum, and the maximal density of region $\rho_{\text{max},i}$ is the density where the flow becomes zero and region i gridlocks.

To model the traffic dynamics outlined above in this framework, we consider behaviors $\mathcal{B} \in \mathcal{L}^{m+p}$ over a signal $w = \text{col}(u, y) \in \mathbb{R}^q$ divided into an input u of dimension $m = l + p^2$ and an output y of dimension p . As output we consider the traffic density $\boldsymbol{\rho} \in \mathbb{R}^p$ in the p regions of the traffic network. The inputs u are further subdivided into controllable inputs $\boldsymbol{\lambda} \in \mathbb{R}^l$ (the fractions of active phase of the controlled intersections) and uncontrollable inputs $\boldsymbol{d} \in \mathbb{R}^{p^2}$ (the demands of all possible origin-destination region pairs). This leads to

$$\begin{aligned} u(t) &:= \text{col}(\boldsymbol{\lambda}(t), \boldsymbol{d}(t)) \in \mathbb{R}^m, \\ y(t) &:= \boldsymbol{\rho}(t) \in \mathbb{R}^p, \end{aligned}$$

and a signal $w = \text{col}(u, y) \in \mathbb{R}^q$ of dimension $q = l + p + p^2$. The dynamics of the signal are described by a non-linear function h relating, for example, the density or flow in one time instant with those in the next time instant. Common choices for h include partial differential equations, discretised by first or second order methods [89, 90]. In this work, we do not concern ourselves with the choice of a specific model for h , but consider trajectories of the corresponding quantities and construct a high-dimensional linear approximation f of h based solely on data. Let $T, T_{\text{ini}} \in \mathbb{N}$ with $T_{\text{ini}} < T$ and a fixed $t \in \mathbb{T}$, consider a finite output trajectory $y|_{[t-T_{\text{ini}}, t]} = (y(t - T_{\text{ini}}), \dots, y(t))$, and input trajectory $u|_{[t-T_{\text{ini}}, t]} = (u(t - T_{\text{ini}}), \dots, u(t))$. We then consider a linear function $f : (\mathbb{R}^p)^{T_{\text{ini}}} \times (\mathbb{R}^m)^{T_{\text{ini}}} \rightarrow \mathbb{R}^p$ of the following form

$$y(t+1) = f(y|_{[t-T_{\text{ini}}, t]}, u|_{[t-T_{\text{ini}}, t]}), \quad (3)$$

and introduce the behavior associated with the traffic density as

$$\mathcal{B}_{\boldsymbol{\rho}} = \left\{ (y, u) \in \mathbb{R}^{(l+p+p^2)T_{\text{ini}}} \mid (3) \text{ holds} \right\}. \quad (4)$$

Note that in what follows we never explicitly construct the behavior in 4, but encode the constraint in 3 implicitly using data collected from the system.

To ensure that the trajectories included in the behavior are realistic, additional constraints need to be imposed. Let $T_f \in \mathbb{N}$ be a multiple of the duty cycle time Δ_{dc} and such that $T_{\text{ini}} + T_f \leq T$. We assume that

once the input λ has been chosen, it is kept constant during the duty cycle, that is for a duration Δ_{dc} . This translates into the linear constraint $M\mathbf{u} = \mathbf{0}$, where $M \in \mathbb{R}^{mT_f \times mT_f}$ is used to impose for every $\ell \in \mathbf{I}$ and $k \leq T_f$ the constraint $\lambda_\ell(k+1) = \lambda_\ell(k+2) = \dots = \lambda_\ell(k+\Delta_{\text{dc}})$. We further assume that at every time instant the controllable input has to satisfy the box constraints $\lambda(k) \in [\underline{\lambda}, \bar{\lambda}] \subset [0, 1]^l$, where $\underline{\lambda} = \text{col}(\underline{\lambda}_1, \dots, \underline{\lambda}_l)$ and $\bar{\lambda} = \text{col}(\bar{\lambda}_1, \dots, \bar{\lambda}_l)$. As mentioned before, the values are not allowed to reach the boundary value 1 due to the yellow phase constant duration.

The uncontrollable input \mathbf{d} is assumed to be known and equal to an estimate of the demand $\bar{\mathbf{d}} = \text{col}(\mathbf{d}(t), \dots, \mathbf{d}(t+T_f)) \in \mathbb{R}^{p^2 T_f}$ over the prediction horizon, i.e., $D\mathbf{u} = \bar{\mathbf{d}}$ where the matrix $D \in \mathbb{R}^{mT_f \times p^2 T_f}$ projects to the entries of the input corresponding to the demand. Therefore, the set of constraints for the inputs over the whole prediction horizon reads as

$$\mathcal{U} = \left\{ \mathbf{u} \in ([\underline{\lambda}, \bar{\lambda}] \times \mathbb{R}_+^{p^2})^{T_f} \mid M\mathbf{u} = \mathbf{0}, D\mathbf{u} = \bar{\mathbf{d}} \right\}. \quad (5)$$

Similarly, box constraints on the output are selected to ensure that the density remains non negative and below grid-lock conditions $\rho_{\text{max}} \in \mathbb{R}_+^p$, leading to $y(t) \in [0, \rho_{\text{max}}]$ and a constraint set $\mathcal{Y} := [0, \rho_{\text{max}}]^{T_f}$.

3 Data-enabled predictive control

Consider a LTI system $\mathcal{B} \in \mathcal{L}^{m+p}$, with m inputs and p outputs, assume that data recorded offline from system \mathcal{B} is available. Specifically, assume that an input sequence $u_{\text{d}} = \text{col}(u_{\text{d}}(1), \dots, u_{\text{d}}(T)) \in \mathbb{R}^{mT}$ of given length $T \in \mathbb{N}$ is applied to the system \mathcal{B} and that the corresponding output sequence $y_{\text{d}} = \text{col}(y_{\text{d}}(1), \dots, y_{\text{d}}(T)) \in \mathbb{R}^{pT}$ is recorded. The subscript ‘‘d’’ is used to indicate that these are trajectories of data samples collected offline. Finally, let $T_{\text{ini}} \in \mathbb{N}$ and $T_f \in \mathbb{N}$, with $T_{\text{ini}} + T_f \leq T$, and assume that the sequence $w_{\text{d}} = \text{col}(u_{\text{d}}(t), y_{\text{d}}(t)) \in \mathbb{R}^{(m+p)T}$, for $t \in \mathbb{T} := [1, \dots, T] \subset \mathbb{N}$, satisfies the generalized persistency of excitation condition (see Appendix A). Intuitively, the persistency of excitation condition requires the sequence w_{d} to contain enough information to allow for the systems’ behavior to be reconstructed. We define the *Hankel matrix* of depth $L \in \mathbb{T}$ associated with the finite sequence $w \in \mathbb{R}^{qT}$ as

$$H_L(w) = \begin{bmatrix} w(1) & w(2) & \dots & w(T-L+1) \\ w(2) & w(3) & \dots & w(T-L+2) \\ \vdots & \vdots & \ddots & \vdots \\ w(L) & w(L+1) & \dots & w(T) \end{bmatrix}.$$

Next, we partition the input-output data into two parts, *past data* $(U_{\text{p}}, Y_{\text{p}})$ and *future data* $(U_{\text{f}}, Y_{\text{f}})$. Formally, given the time horizons $T_{\text{ini}} \in \mathbb{N}$ and $T_f \in \mathbb{N}$, we define

$$\begin{pmatrix} U_{\text{p}} \\ U_{\text{f}} \end{pmatrix} = H_{T_{\text{ini}}+T_f}(u_{\text{d}}), \quad \begin{pmatrix} Y_{\text{p}} \\ Y_{\text{f}} \end{pmatrix} = H_{T_{\text{ini}}+T_f}(y_{\text{d}}), \quad (6)$$

where $U_{\text{p}} \in \mathbb{R}^{(mT_{\text{ini}}) \times (T-T_{\text{ini}}+1)}$ is composed of the first T_{ini} block-rows of the matrix $H_{T_{\text{ini}}+T_f}(u_{\text{d}})$ and $U_{\text{f}} \in \mathbb{R}^{(mT_f) \times (T-T_f+1)}$ of the last T_f block-rows, Y_{p} and Y_{f} are attained similarly from $H_{T_{\text{ini}}+T_f}(y_{\text{d}})$. In the remainder, past data, denoted by the subscript ‘‘p’’, is used to implicitly estimate the initial condition of the underlying state, whereas the future data, denoted by the subscript ‘‘f’’, is used to predict future trajectories.

Given $T_f \in \mathbb{N}$, a reference trajectory for the output \hat{y} and the input \hat{u} , most recent past input/output data $w_{\text{ini}} = \text{col}(u_{\text{ini}}, y_{\text{ini}})$, an input constraint set $\mathcal{U} \subseteq \mathbb{R}^{mT_f}$, an output constraint set $\mathcal{Y} \subseteq \mathbb{R}^{pT_f}$, an output cost matrix $Q \geq 0 \in \mathbb{R}^{p \times p}$, a control cost matrix $R \geq 0 \in \mathbb{R}^{m \times m}$, a regularization function $\psi : \mathbb{R}^{T-T_{\text{ini}}-T_f+1} \rightarrow \mathbb{R}$, and parameters $\lambda_y, \lambda_1, \lambda_2 \in \mathbb{R}$, the DeePC algorithm solves the optimisation problem:

$$\min_{u, y, g, \sigma_y} \sum_{k=1}^{T_f} \|y(k) - \hat{y}(t+k)\|_Q^2 + \|u(k) - \hat{u}(t+k)\|_R^2 + \psi(g) + \lambda_y \|\sigma_y\|_1 \quad (7a)$$

$$\text{s.t.} \quad \begin{pmatrix} U_p \\ Y_p \\ U_f \\ Y_f \end{pmatrix} g = \begin{pmatrix} u_{\text{ini}} \\ y_{\text{ini}} \\ u \\ y \end{pmatrix} + \begin{pmatrix} 0 \\ \sigma_y \\ 0 \\ 0 \end{pmatrix}, \quad (7b)$$

$$u \in \mathcal{U}, y \in \mathcal{Y}. \quad (7c)$$

Solving (7) generates a trajectory of future inputs, u , and outputs, y , for the next T_f time steps. The equality constraint ensures that the trajectories are compatible with the system dynamics (encoded in the data matrix) and the most recent data collected from the system and stored in u_{ini} and y_{ini} . The regularization term $\psi(g)$ is defined as

$$\psi(g) := \lambda_1 \|(I - \Pi)g\|_2^2 + \lambda_2 \|g\|_1 \quad \text{where } \Pi = \begin{bmatrix} U_p \\ Y_p \\ U_f \end{bmatrix}^\dagger \begin{bmatrix} U_p \\ Y_p \\ U_f \end{bmatrix}.$$

The first addend $\|(I - \Pi)g\|_2^2$ computes the orthogonal projection on the kernel of the first three block equations of (7b), while the second addend $\|g\|_1$ computes a low-rank approximation on the column space of H . Together the two terms greatly improve the performance of DeePC in non-linear settings, for more details on the regularization action the interested reader is referred to [91]. The slack variable σ_y relaxes the constraint to ensure that it remains feasible; it is penalised by the regularization term $\lambda_y \|\sigma_y\|_1$ to keep the constraint violation small. The set membership constraints (7c) ensure that the decision variables remain within the admissible input domain \mathcal{U} and the physically consistent output domain \mathcal{Y} . The cost (7a) trades off tracking accuracy $\|y(k) - \hat{y}(t+k)\|_Q^2$ and control effort $\|u(k) - \hat{u}(t+k)\|_R^2$ with respect to the reference values \hat{y} and \hat{u} . Once the optimisation problem is solved, the first element of the trajectory u is applied to the system, a new measurement is collected, the vectors u_{ini} and y_{ini} are updated with this new information and the process is repeated in a receding horizon fashion. The process is summarised in Algorithm 1.

Algorithm 1 DeePC

Input: Future time horizon $T_f \in \mathbb{N}$, a reference trajectory for the output $\hat{y} = (\hat{y}_0, \hat{y}_1, \dots) \in (\mathbb{R}^p)^{\mathbb{N}}$ and the input $\hat{u} = (\hat{u}_0, \hat{u}_1, \dots) \in (\mathbb{R}^m)^{\mathbb{N}}$, past input/output data $w_{\text{ini}} = \text{col}(u_{\text{ini}}, y_{\text{ini}}) \in \mathcal{B}_{|[1, T_{\text{ini}}]}$, an input constraint set $\mathcal{U} \subseteq \mathbb{R}^{mT_f}$, an output constraint set $\mathcal{Y} \subseteq \mathbb{R}^{pT_f}$, a output cost matrix $Q \in \mathbb{R}^{p \times p}$, a control cost matrix $R \in \mathbb{R}^{m \times m}$, a regularization function $\psi : \mathbb{R}^{T - T_{\text{ini}} - T_f + 1} \rightarrow \mathbb{R}$, and parameter $\lambda_y \in \mathbb{R}$.

- 1: Compute the minimizer g^* of (7).
 - 2: Compute optimal input sequence $u^* = U_f g^*$.
 - 3: Apply optimal input sequence $(u_t, \dots, u_{t+j-1}) = (u_1^*, \dots, u_j^*)$ for some $j \leq T_f$.
 - 4: Set t to $t+j$ and update u_{ini} and y_{ini} to the T_{ini} most recent input/output measurements.
 - 5: Return to 1.
-

For our traffic model we use the quantity ρ_{cr} estimated from the regions MFDs in Section 2.3 as constant output reference \hat{y} . In (7), we minimize the distance between the regions' density ρ_i and critical $\rho_{\text{cr},i}$ at each time step. The MFD (and hence the reference \hat{y}) can initially be estimated using data from the historical operation of the system. We note, however, that this data implicitly depends on the policy used to control the intersections. Since our goal is to change this policy, it is conceivable that when the system is operating under the DeePC algorithm, its MFD will change. This effect can be mitigated by re-estimating the MFD online with data collected under the DeePC policy, the reference \hat{y} can be recomputed and the process repeated. One should be careful to ensure the stability of the algorithm as considering a non-continuous

trajectory can be problematic. For the sake of a fair comparison among the different control policies explored in Section 4, we decided to leave this online optimization of the control scheme for future research.

The reference value of the inputs $\hat{u} := \text{col}(\hat{\lambda}, \hat{d})$ is composed by two parts, the first is the default green time to duty cycle time ratio $\hat{\lambda}$, which is the ratio that the traffic lights would exhibit given their phase specification if no dynamic control were to be applied. The latter is exogenous and set equal to \bar{d} according to (5). In the cost function in (7), the matrices R and Q are chosen positive definite. Note that the components of $\|u - \hat{u}\|_R$ associated with \bar{d} are always equal to zero due to the chosen reference and the constraints on u . Finally, the regularization term ψ is chosen as in [46]. Note that in general the optimization problem only requires convexity of the cost function.

4 Simulation

We use SUMO to simulate traffic dynamics at a microscopic level and generate realistic data. An implementation of the controller then interacts with the simulation in closed-loop through a custom interface built on TraCI. The interface code as well as the simulations networks are openly available at <https://github.com/AlessioRimoldi/TrafficGym>. The routing of each vehicle is recomputed periodically using the A* algorithm, accounting for current traffic conditions. Once a vehicle reaches its destination, it is removed from the simulation. We consider two different traffic networks, a lattice network and the urban traffic network of Zürich. We use a simulation where the traffic lights follow the standard static cycle specified by the SUMO configuration as a baseline, in this case no input is given to the simulation. We further compare DeePC with the MPC formulation detailed in [76], in this work the authors first devise a linear program formulation to solve the finite-time optimal perimeter flow control problem. The traffic dynamics are described first using a non-linear model derived from the MFD, the linear formulation is then achieved as a linearization of this model, employing a piecewise approximation of the MFD. The linear program is then solved in a rolling horizon using a feedback MPC framework, for completeness we report the MPC formulation in Appendix C. The parameters used by the controllers can be found in Appendix D.

4.1 Lattice network simulation

The lattice network is composed of 104 two-way roads and 64 intersections. Figure 7b shows the network partitioned into two regions emulating a city center and its suburban area, connected by 8 roads. We refer to these two regions as the inner and outer region respectively.

Actuators and demand profile We selected twelve traffic lights to be used as actuators, eight of which are at the boundary between the two regions and can be used to perform classical perimeter control, while the remaining are in the inner region to manage the internal dynamics, see Figure 7b. All controlled intersections have four approaches. We consider a standard duty cycle time of $\Delta_{dc} = 90$ s, with two green phases lasting 42 seconds, plus two yellow phases lasting 3 seconds. The demand profile in Figure 7a has two distinct peaks, spanning two hours with a total of 6149 vehicles. Each vehicle is generated at the external boundary of the outer region, and assigned a destination edge inside the inner region. This makes the demand unidirectional, from the outer to the inner region, no additional vehicles are generated.

Results The evolution of the density and flow in the inner region is shown in Figure 8. The baseline simulation reaches a state of grid-lock shortly before the end of the first peak of demand, leading to high travel times. Due to the congestion only 4636 vehicles complete their trip. On the other hand, control of the traffic lights via DeePC and MPC prevents grid-lock, maintaining a stable flow throughout the length of the simulation. Table 1 shows the average travel time and emissions metrics over the number of vehicles that completed their trip, we observe DeePC performing better than MPC on all metrics. We conjecture that this improvement in performance is due to the implicit model defined by the Hankel matrix included in DeePC capturing the underlying traffic dynamics better than the linear formulation used by MPC, note that both models perform a linear approximation.

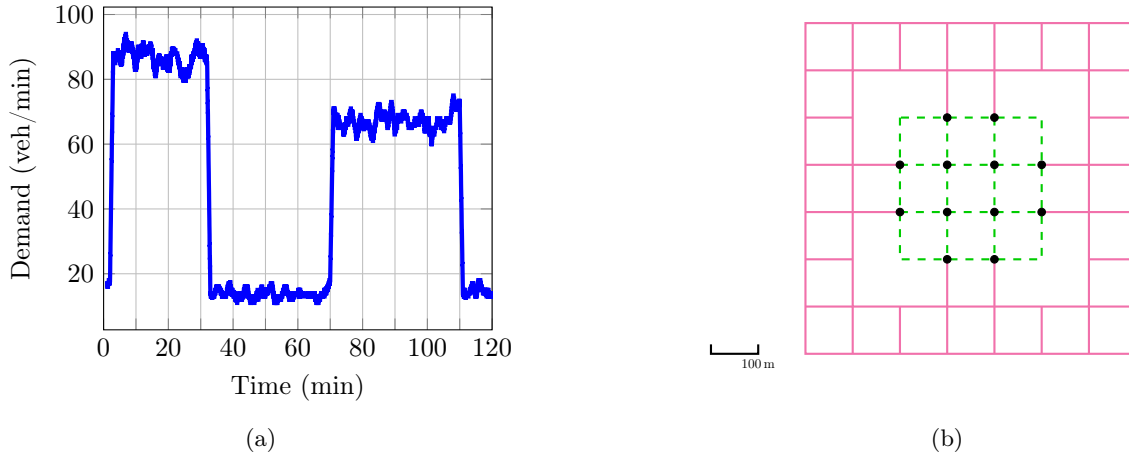


Figure 7: Left panel shows the demand profile, the vehicles move from the outer to the inner region. The network is partitioned into the *outer region* (solid magenta line) and in *inner region* (dashed green line). Black dots represent the controlled traffic lights.

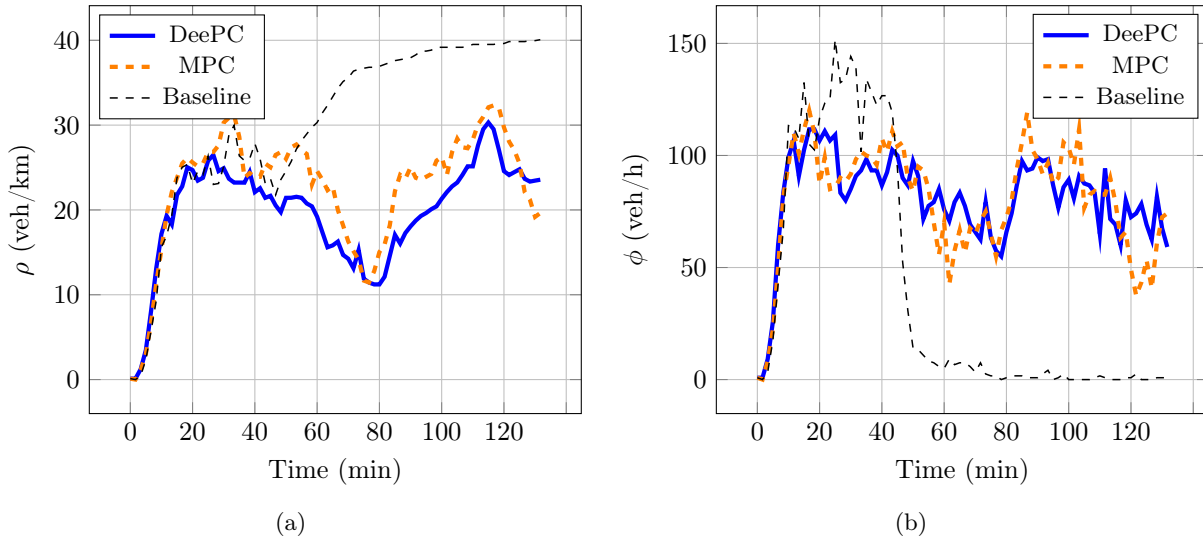


Figure 8: Evolution of the density (left panel) and flow (right panel) in inner region of the lattice network.

4.2 Zürich simulation

We now present the simulation of Zürich, Switzerland, built on a digital twin developed at Transcality [92]. The urban traffic network of the city comprises almost 15,000 roads with different number of lanes, connecting approximately 7,000 intersections, see Figure 9. The demand profile is estimated using real data measured by the city loop detectors. In our experiments, we consider the period corresponding to the evening traffic peak, spanning the hours from 16:00 to 21:00. During this surge in demand, the network serves more than 170,000 vehicles. Figure 9b shows the traffic regions obtained by applying a parallelized version of the snake clustering algorithm described in [79], see Appendix B. Remarkably, the identified regions closely resemble the real districts of the city, for example, one can recognize the Wiedikon area in red. This similarity is due to the use of real data in demand and traffic network modeling.

	Baseline	MPC	DeePC	% variation
Travel Time (min)	27.5	26.03	24.93	- 9.34%
Waiting Time (min)	25.33	22.24	21.39	- 15.55%
CO Emissions(g)	259.65	239.59	229.5	- 10.92%
CO2 Emissions (g)	4,351.16	4,084.12	3,917.79	- 9.95%
HC Emissions (g)	1.28	1.19	1.14	- 10.37%
PMx Emissions (g)	0.11	0.1	0.1	- 8.95%
NOx Emissions (g)	1.98	1.86	1.78	- 10.10%
Fuel consumption (ml)	1,387.91	1,302.73	1,249.67	- 9.96%
Trips completed	4,636	5,377	5,642	+ 21.69%

Table 1: Average metrics for the lattice network

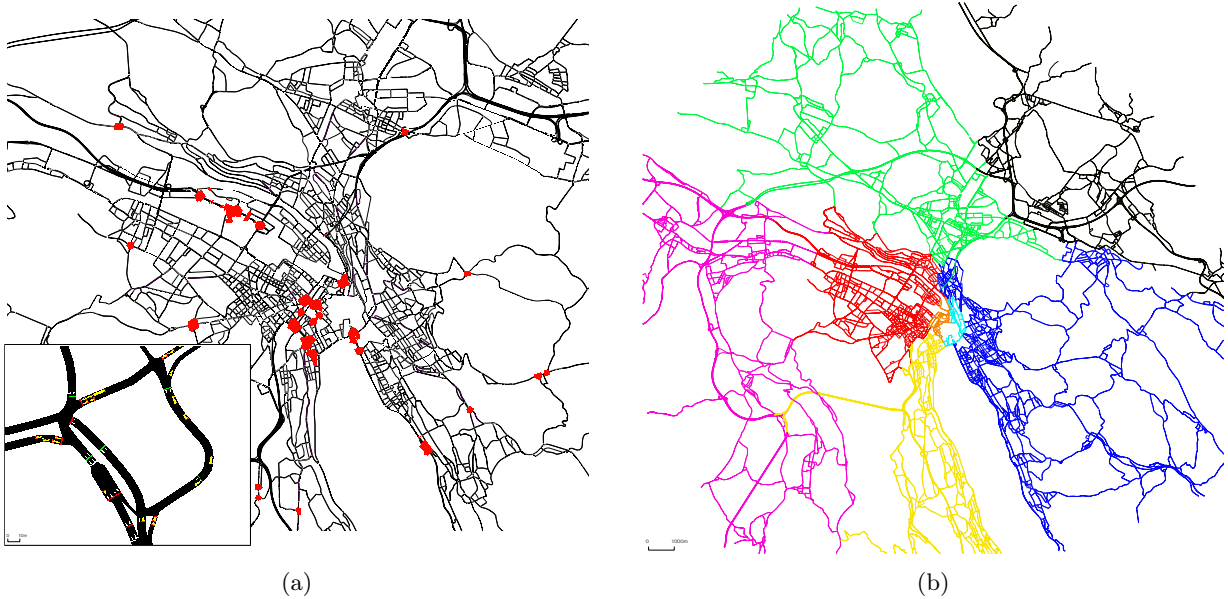


Figure 9: Left panel shows the Zürich urban traffic network embedded in SUMO. Actuated intersections are highlighted in red. In the corner, one of the controlled intersections, Bellevue. Right panel shows the region partitioning found using the snake clustering algorithm, the Wiedikon region is highlighted in red.

Actuators and demand profile The network comprises over 800 intersections with controllable traffic lights. To ensure the simulation is realistic, we took advantage of the expert knowledge of the traffic engineers of the city of Zürich and selected the 47 actuators that the municipality is currently using as actuators [93], the position of these actuators can be seen in Figure 9a. Although the phase definition depends on the topology of the intersection, all actuated traffic lights have a duty cycle time of $\Delta_{dc} = 72 s$. One of the actuated intersections can be seen in Figure 9a. The demand profile directed to the Wiedikon region (highlighted in red in Figure 9b) is shown in Figure 10, where the color coding of the plot matches the one of Figure 9b. The data is collected during a day of average congestion in the city, therefore the baseline simulation does not reach a grid-lock.

Results The comparison of density and flow under control of DeePC and MPC for the Wiedikon region, highlighted in red in Figure 9b, can be seen in Figure 11. Figure 11a additionally shows the value of the critical density ρ_{cr} of the region. Due to the high variability of the flow, a moving average filter of window

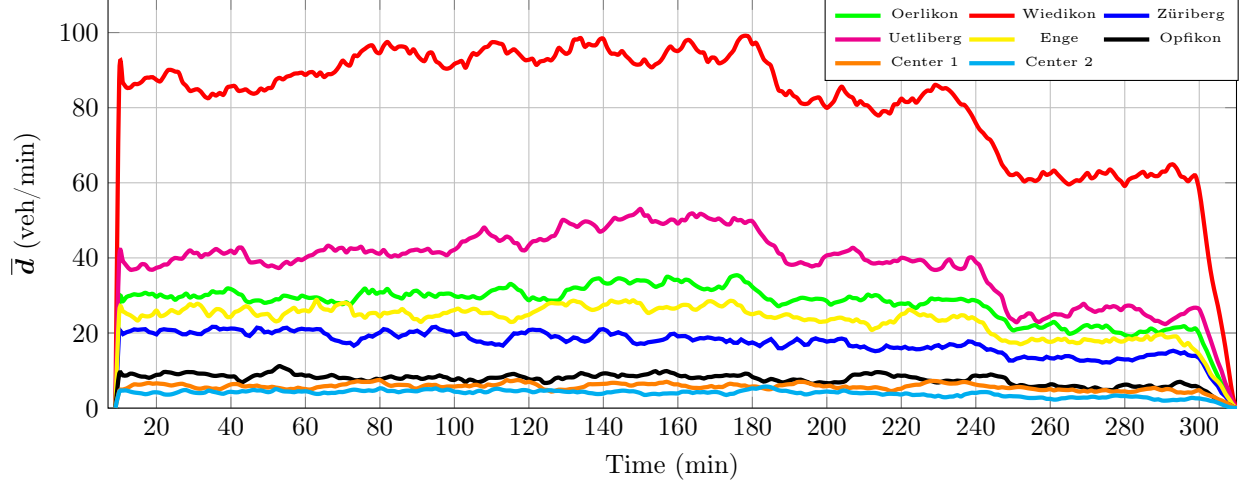


Figure 10: The demand profile directed to the Wiedikon region broken down by region of origin. The color coding used matches the one in Figure 9b.

10 has been applied to the flow time series to aid comprehension of plot 11b. The behavior of this region is representative as all the other regions in the network behave similarly. Also in this network DeePC is able to outperform MPC and improve traffic conditions leading to a 18% decrease in travel time, see Table 2. This suggests that the data-generated approximation of the relation between traffic light control and density succeeds in capturing traffic dynamics effectively. This supports the conjecture made in Figure 5 that the relation between the two quantities is linear. The MPC controller also achieves an improvement in travel time which, however, remains higher than under the DeePC policy. One reason for this is that the MPC solves the perimeter control problem by computing the optimal flows, referring back to Figure 5, we know that the relation between the traffic light control and the flow to be non-linear, this leads to an inaccurate linear approximation. Moreover, both algorithms perform a linearization of the traffic dynamics providing a fair comparison, however, since the MPC formulation computes first the optimal flows between regions, a mapping between these flows and the actuators is then needed to assign the inputs to the right actuators. If the actuators are placed on the borders between regions constructing this mapping is trivial. If, however, the actuators are allowed to be anywhere in the network, this makes constructing the mapping more difficult, as one actuator could be responsible for the modulation of multiple flows directed to different regions. In practice, each actuator must receive just one input at a time, this requires it to be assigned to a single flow which introduces an approximation error and degrade performance. DeePC avoids this problem as the mapping is defined implicitly by the Hankel matrix leading to better performance. Because updating the control at every duty cycle may be undesirable in practice due to the frequent changes in phase duration, we also evaluate DeePC with longer control periods. Specifically, we simulate control with a period of 1,3 and 6 Δ_{dc} , this means that we compute the optimal green times and keep them constant for 1,3 and 6 duty cycles before recomputing. The evolution of the density under this control can be seen below in Figure 12. Note that as we control less often, the performance of the algorithm degrades and approaches the baseline. Table 2 shows the effects on average travel time and emissions metrics of with the different control periods.

Input analysis To illustrate the control decision made by the DeePC algorithm, we further analyze the time series of the optimal inputs $\lambda(t)$ found by DeePC. To this end we collect the time series of the inputs in a matrix $\Lambda \in \mathbb{R}^{l \times T}$ and perform a Principal Component Analysis (PCA) over this matrix using $k = 10$ components. PCA is used to find patterns high dimensional data, it works by finding the eigenvectors, named principal components, of the covariance matrix $\Sigma = \frac{1}{T-1} \Lambda^T \Lambda \in \mathbb{R}^{T \times T}$ constructed from data. In this setting each eigenvalue $\text{eig}_i(\Sigma)$ of the covariance matrix represents the amount of variance in the data explained

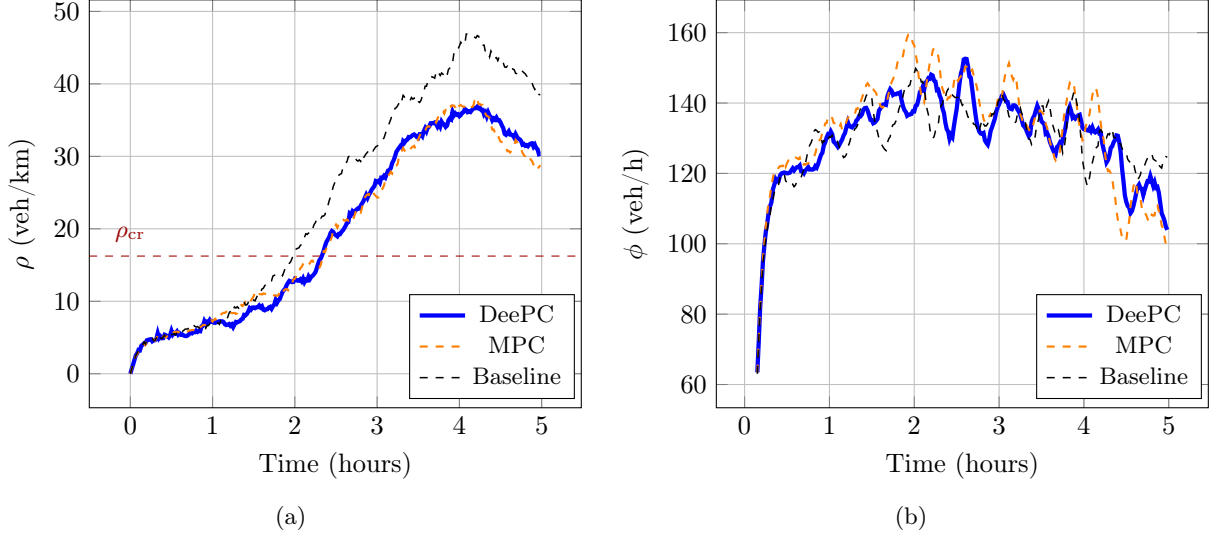


Figure 11: Evolution of density (left panel) and flow (right panel) under control of DeePC and MPC for the Wiedikon region. The critical density value ρ_{cr} (red dashed line) is reported in the left panel, the line represents the threshold for congestion of the system.

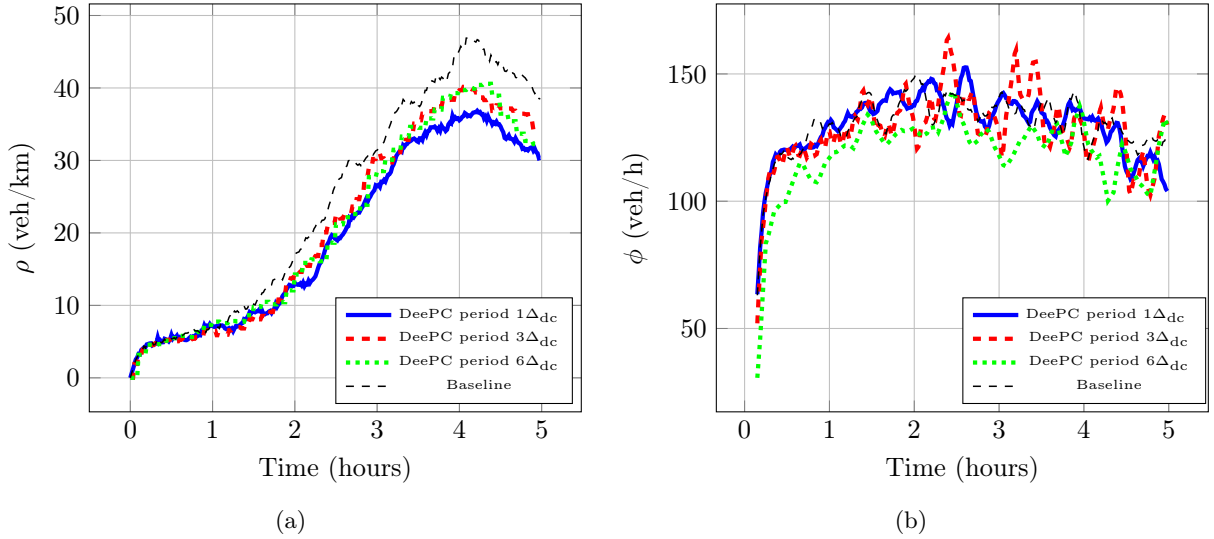


Figure 12: Evolution of density (left panel) and flow (right panel) under control of DeePC with different periods for the Wiedikon region.

by it corresponding principal component. The explained variance ratio associated to the i -th eigenvalue is defined as

$$EVR_i := \frac{\text{eig}_i(\Sigma)}{\sum_j^k \text{eig}_j(\Sigma)} \quad (8)$$

These ratios represent the percentage of the dataset variance each principal components accounts for. Table 3 shows that the first principal component accounts for almost 50% of the total input variation in all the 47 actuators, with the second and third components accounting for 10.3% and 5.1% respectively. In other words, the first component is describing a strong global pattern that the controller used to adjust the input

Table 2: Average Metrics Zürich

	Baseline	DeePC $6\Delta_{dc}$	DeePC $3\Delta_{dc}$	MPC	DeePC $1\Delta_{dc}$	
Travel Time (min)	45.23	39.07	37.94	38.51	37.05	-18.08%
Waiting Time (min)	28.27	23.31	22.62	23.07	21.87	-22.60%
CO Emissions(g)	16.91	15.84	15.41	16.14	15.67	-7.33%
CO2 Emissions (g)	4,992.15	4,379.17	4,253.91	4,338.89	4,184.46	-16.17%
HC Emissions (g)	0.11	0.11	0.10	0.11	0.11	-0.00%
PMx Emissions (g)	0.22	0.21	0.21	0.21	0.21	-4.54%
NOx Emissions (g)	1.91	1.67	1.62	1.66	1.60	- 16.23%
Fuel consumption (ml)	1,618.41	1,419.69	1,379.07	1,406.63	1,356.56	- 16.17%
Trips completed	176,821	177,555	178,143	176,980	178,035	+0.74%

Component	PC1	PC2	PC3	PC4	PC5	PC6	PC7	PC8	PC9	PC10
EVR	0.477	0.103	0.051	0.037	0.033	0.026	0.022	0.021	0.020	0.018

Table 3: Explained variance ratios of the components, each value represents the percentage of variation in the control input that can be explained by the corresponding principal component.

to the actuators. Figure 13a shows the evolution of the value of the first three principal components during the simulation. We observe that, while the second and the third components values remain relatively stable, the first component starts with positive values and then around two and a half hours experiences a rapid change to negative values. This suggests a change in the environment in which DeePC is operating at that time, that led to a change the global pattern. Indeed, by observing Figure 11a we can see that exactly around that time the traffic density starts to increase rapidly, approaching the line defined by the reference trajectory ρ_{cr} , once the line is crossed the network enters a state of congestion, which triggers the observed inversion in the global input pattern.

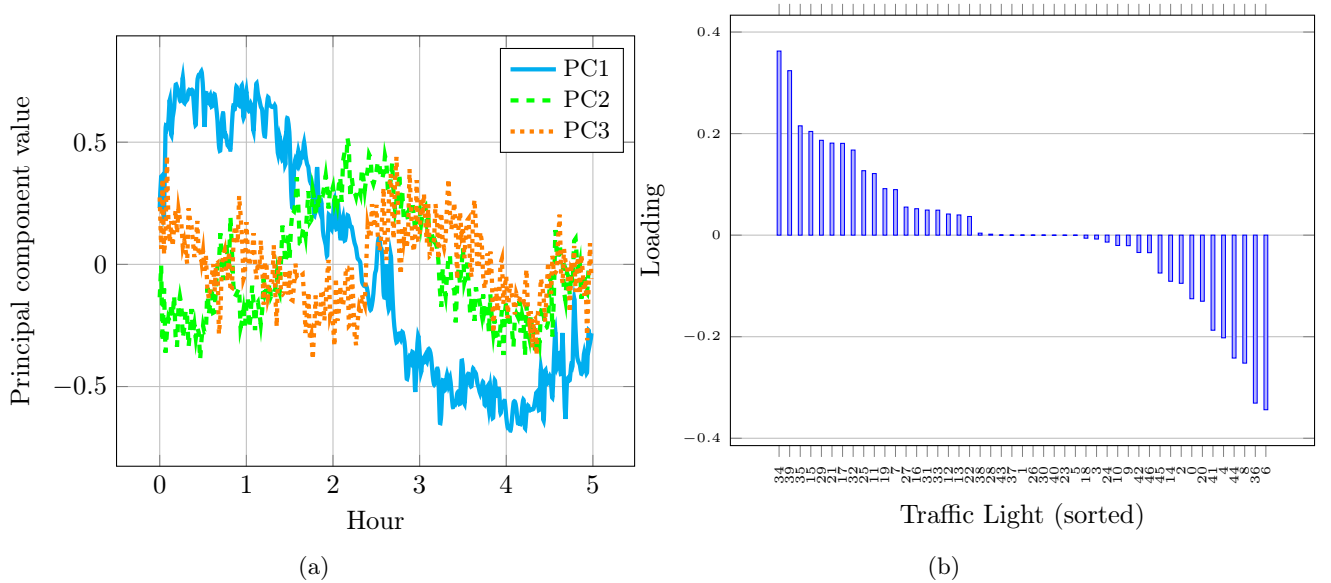


Figure 13: Left panel shows the evolution of the first three PCA components. Right panel shows the loadings value associated to PC1.

Figure 13b, shows a bar plot of the loading values, or actuator weights, associated to the first principal component sorted in descending order. The magnitude of a loading gives information on the amount of variation in the input that the corresponding actuator is responsible for, with positive values indicating positive correlation with the pattern and the negative ones negative correlation. This allows us to identify which actuators had the most influence over the traffic conditions. We can see that few actuators have large absolute loading value, allowing us to pinpoint the geographical locations of these influential actuators; their positions can be seen in Figures 14. We observe the positively correlated actuators to be positioned on key access points to the city, such as highway exits, while the negatively correlated actuators cluster around the city center.

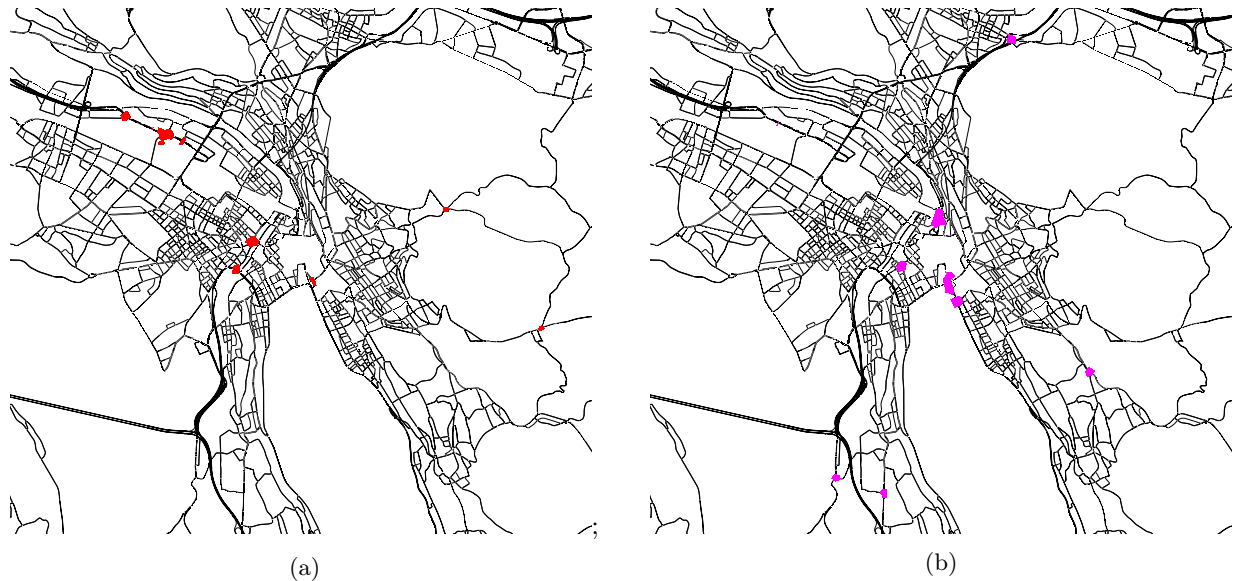


Figure 14: Positions of the highly influential actuators. Left panel shows the positions of the ten highest loading value (positively correlated) actuators highlighted in red. Right panel shows the positions of the ten lowest loading values (inversely correlated) actuators highlighted in magenta.

Figures 15 show the control input time series of the two most important positively and negatively correlated actuators. Note that the time series are indeed correlated with the first component evolution in Figure 13a. Most importantly, the positively correlated actuators start with higher green times, and then change to lower green times, while the opposite is true for the negatively correlated actuators. This is reasonable, higher green times are allowed until the congestion threshold ρ_{cr} is reached, after that the control regime changes to lower green times. Given that the positively correlated actuators are placed at key access points to the city, lower green times lead to less people accessing the inner regions city at a time, giving time for the current demand to clear aided by the higher green times provided by the negatively correlated actuators in the city center.

Macroscopic fundamental diagram comparison Another way to interpret the effect of the control policy of DeePC is to compare the MFD obtained under its influence with the one obtained under the static baseline policy. Figure 16 shows two data distributions, each point representing a density-flow pair for the Wiedikon region. The first distribution (gray dots) is data collected under the static cycle specified by the SUMO configuration with no input passed to the simulation, that is the baseline simulation used in Figures 11, 12. The second distribution (blue squares) is data collected under the DeePC control policy with period $1 \Delta_{dc}$, that is computing the control action for every duty cycle. Note that the data distribution collected under DeePC remains at lower densities compared to the baseline data distribution while maintaining a

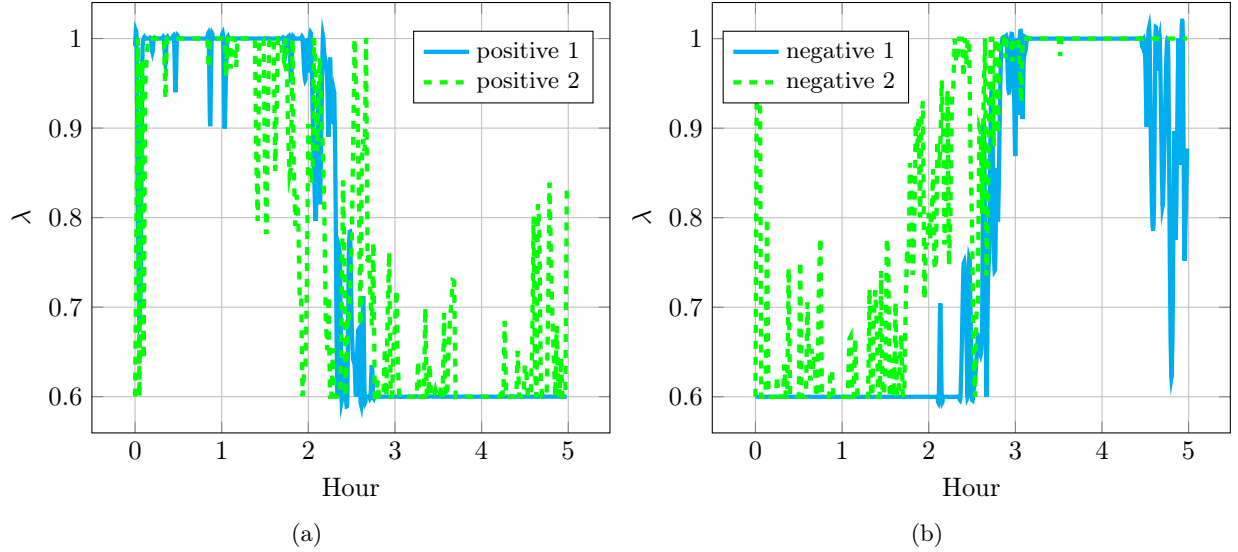


Figure 15: Input time series of the two most influential actuators respectively positively (left panel) and negatively correlated actuators.

comparable flow, this is reflected also in Figure 11. Since the average flow of a region can be expressed as $\phi_i = \rho_i v_i$ where v_i is the average speed of the vehicles in the region, Figure 16 suggests that to maintain the same level of flow as the baseline data distribution at a lower density, the vehicles must be moving at a higher average speed, leading to a decrease in travel time with respect to the baseline. The MFDs corresponding to the two data distributions are retrieved by fitting two polynomials of 4-th degree (black and blue lines), the critical density ρ_{cr} is computed for both distributions and shown in Figure 16. We note that the two values do indeed differ from one another by a factor of 2.5 vehicles per kilometer, with the DeePC distribution being more weighted towards the origin, this bias did not noticeably influence performance.

In conclusion, using DeePC to control large traffic systems presents several advantages. The formulation requires only the solution of a quadratic problem that can be efficiently solved in real time using modern solvers. Modeling efforts are substituted by a data collection step and estimation of the critical densities. Thanks to this, it is able to exploit the seemingly linear relation between traffic lights control and densities, bypassing the non-linear relation between traffic light control and flows.

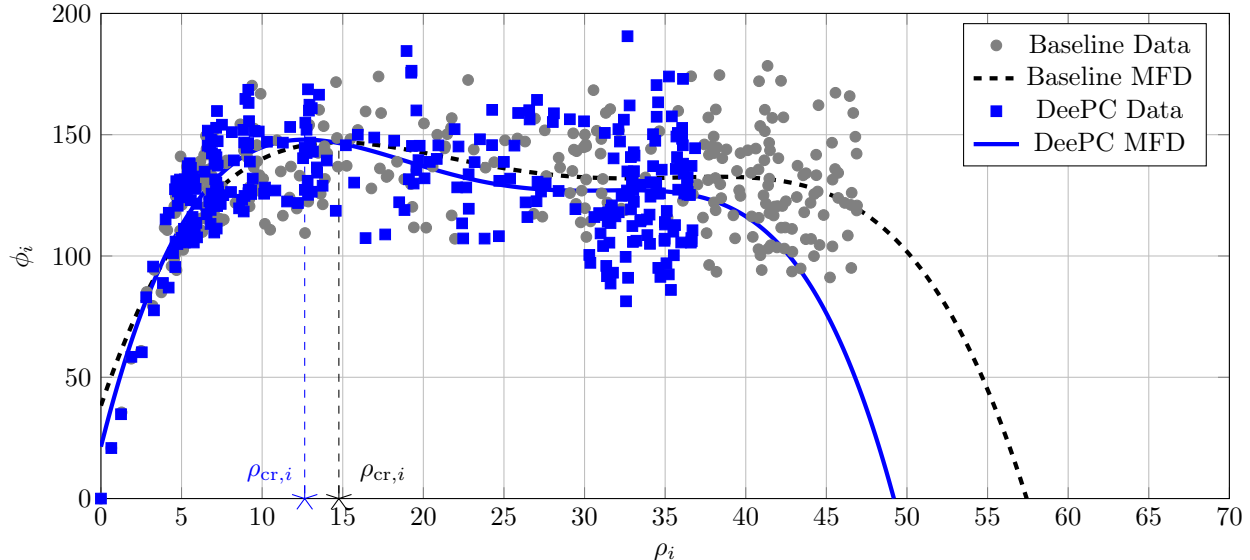


Figure 16: Comparison between the density-flow data distribution of Wiedikon obtained under the static control policy (gray dots) and under the DeePC control policy (blue squares). The MFDs and critical densities ρ_{cr} are shown in the corresponding colors for both distributions.

5 Conclusions and future research

In this work, we have shown that the DeePC algorithm is able to effectively solve the ITSCP leveraging data. We modeled traffic dynamics using behavioral systems theory and obtained a flexible and scalable formulation useful to optimize key metrics (e.g., CO₂ emissions and travel times) for large non-linear traffic systems. Our methodology has several advantages, first, the modeling efforts that are usually required upfront to solve the ITSCP are substituted by a much simpler data collection procedure. Second, the formulation is flexible, allowing for seamless incorporation of different kinds of data and actuators. Third, our methodology does not require that the actuators used to be placed at, or close to, the perimeter of the regions. In other words, our methodology formally generalizes standard perimeter control, through the Hankel matrix an implicit mapping is created between the actuators and the aggregate dynamics of the network. Therefore, we resolve to normal perimeter control if the actuators are placed at the region boundaries.

The method comes with some drawbacks too. First, when dealing with non-linear systems, one cannot be sure that the Hankel matrix spans the whole behavior of the system, even if it satisfies the rank conditions needed for persistency of excitation. This leads to the fact that, depending on the distribution of the data collected from the system, we may not be able to obtain a satisfactory control policy from every Hankel matrix. This means that a Hankel matrix will only be able to represent the system appropriately when the conditions of the system, i.e., the exogenous demand, are close enough to the conditions in which the data were collected. This leads to a number of new research directions that could be explored in order to make this method more robust to different conditions. For example, one could design a data collection pipeline aimed at mapping multiple behaviors of the non-linear system and then either aggregate behaviors into a single Hankel matrix or build a library of Hankel matrixes and choose through some criterion the matrix that best matches the current conditions. Another challenging problem regards scalability, as the dimension of the optimization problem scales with the number of actuators. A possible solution is to distribute the DeePC algorithm via alternating projections [94]. As final words, DeePC is a promising new tool that has been proven to work in a variety of applications, in this paper we explored how it can be applied to perform urban traffic control by solving the ITSCP problem, while the results are promising many research directions have been opened for future work.

A Preliminaries

The following preliminary discussion closely follows the one in [10] and it is reported here to render this work self-contained.

The restriction of a sequence over an interval gives rise to the cut operator. Formally, given $w \in (\mathbb{R}^q)^\mathbb{T}$ and $L \in \mathbb{T}$, the *cut operator* is defined as

$$w|_L = (w(1), \dots, w(L)) \in (\mathbb{R}^q)^L.$$

For infinite trajectories, the definition holds verbatim with $w \in (\mathbb{R}^q)^\mathbb{N}$ and $L \in \mathbb{N}$. Applied to a set \mathcal{W} of (finite or infinite) trajectories, the cut operator acts on all elements in the set giving rise to the *restricted set* $\mathcal{W}|_L = \{w|_L : w \in \mathcal{W}\}$.

Shifting elements of a sequence give rise to the shift operator. Formally, given $w \in (\mathbb{R}^q)^\mathbb{T}$ and $\tau \in \mathbb{T}$, the *shift operator* is defined as

$$\sigma^{\tau-1}w = (w(\tau), \dots, w(T)) \in \mathbb{R}^{q(T-\tau+1)}.$$

For infinite trajectories, the shift operator is defined as $w \mapsto \sigma^{\tau-1}w$, with $\sigma^{\tau-1}w(t) = w(t + \tau - 1)$, for any $\tau \in \mathbb{N}$. Applied to a set \mathcal{W} of (finite or infinite) trajectories, the shift operator acts on all elements in the set giving rise to the *shifted set* $\sigma^\tau\mathcal{W} = \{\sigma^\tau w : w \in \mathcal{W}\}$. For finite-length time series, the *unit shift operator*, defined as $\sigma(\cdot) = \sigma^1(\cdot)$, can be applied at most $T - 1$ times.

Given $m \in \mathbb{N}$ and a permutation matrix $\Pi \in \mathbb{R}^{q \times q}$, the map $w \mapsto \Pi w = (u, y)$ defines a *partition* of $w \in (\mathbb{R}^q)^\mathbb{N}$ into the variables $u \in (\mathbb{R}^m)^\mathbb{N}$ and $y \in (\mathbb{R}^{q-m})^\mathbb{N}$. The map is an *input-output partition* of a system Σ if u is *free*, *not anticipated*, and *causal* [95], in which case u is the *input* and y is the output of Σ . The reader is referred to [45, Section 6] and [95] for further detail.

The structure of an LTI system is characterized by a set of integer invariants known as *structure indices* [45]. The most important ones are the *number of inputs* m , *number of outputs* p , the *lag* ℓ , and the *order* n , see, [45, Section 7] for definitions. Every finite-dimensional LTI system admits a minimal representation and can be described by the equations

$$\sigma x = Ax + Bu, \quad y = Cx + Du, \tag{9}$$

where $\begin{bmatrix} A & B \\ C & D \end{bmatrix} \in \mathbb{R}^{(n+p) \times (n+m)}$ and m , n , and p are the number of inputs, the order, and the number of outputs, respectively.

The *order* of an LTI system $\mathcal{B} \in \mathcal{L}^q$ is the smallest $n \in \mathbb{N}$ among all (minimal) state-space representations (9) and the *lag* is the smallest $\ell \in \mathbb{N}$ such that in a (minimal) state-space representation the *observability matrix*

$$O_\ell = \begin{bmatrix} C \\ CA \\ \vdots \\ CA^{\ell-1} \end{bmatrix}$$

is full rank.

Given a trajectory $w_d \in \mathbb{R}^{qT}$ of a system $\mathcal{B} \in \mathcal{L}^q$, it is possible to derive a non-parametric representation of its finite-horizon behavior using raw data. We summarize a version of this principle known in the control theory literature as the *fundamental lemma* [96].

Lemma 1 [97, Corollary 19] *Consider a system $\mathcal{B} \in \mathcal{L}^q$ with lag $\ell \in \mathbb{N}$ and a trajectory of the system $w_d \in \mathcal{B}|_{[1,T]}$. Assume $L > \ell$. Then $\mathcal{B}|_{[1,L]} = \text{im } H_L(w_d)$ if and only if*

$$\text{rank } H_L(w_d) = mL + n, \tag{10}$$

where n and m are the order and the number of inputs of the system, respectively.

Lemma 1 is a key result in data-driven control [44]. It characterizes all trajectories of a given length of an LTI system in terms of the image of a Hankel matrix, which, in turn, can be constructed directly from raw data. This foundational principle can be adapted in various ways to suit different assumptions, see the recent survey [44]. Remarkably, non-parametric representations have found practical use in data-driven control even when dealing with *non-linear* systems [98, 99].

The rank condition (10) is known as the *generalized persistency of excitation* condition [97]. Note that upper bounds on the structure indices of \mathcal{B} are necessary to check this condition from data. Alternatively, the rank condition (10) can be guaranteed to hold for controllable systems if a certain rank condition on the inputs holds [96].

B Region partitioning

When considering large-scale traffic networks of a whole city, researchers often rely on aggregate models describing the flow of vehicles among different regions [39, 76]. We adopt a similar approach, dividing a city into traffic-wise homogeneous regions to decrease the number of variables taken into consideration. Aggregate descriptions such as the MFD also reduce the variability in the data, which in turn smoothens the dynamics of the system and renders it more suited to linear approximations such as the one performed by DeePC. In this section we provide the details on how to achieve a partitioning such as the seen in Figure 9b.

We run a single simulation without any actuation acting on the traffic lights and collect roadwise density data. We then average the data over the simulation duration and assign to each road its average traffic density. We use this data to run the Snake clustering algorithm [79]. It is possible to parallelize the first two steps of the algorithms presented in [79], that is **A.** Running the snakes and **B.** computing similarities. This is especially necessary for step **B.** as it scales with a complexity of $\mathcal{O}(n^2)$. Assume to have $n \in \mathbb{N}$ roads in a city collected in a set \mathcal{X} each equipped with its traffic density averaged over time $\hat{\rho}$. Given a depth $m \in \mathbb{N}, m < n$. We present below the pseudocode for the parallel implementation of the algorithm

Algorithm 2 Parallel snake clustering

Input: A set of roads \mathcal{X} with cardinality n , $\mathcal{N}(A)$ the set of neighbouring roads of a set A , a maximal snake length $m \leq n$

A. Running the snakes

parallel do

$S_x \leftarrow x$

while $\text{Size}(S_x) < m$ **do**

$S' = \mathcal{N}(S_x)$

$s^* = \{s \mid \min_{s \in S'} \text{var}(S_x \cup s)\}$

$S_x \leftarrow [S_x, s^*]$

end while

end parallel

B. Computing similarities

Initialize ϕ

Initialize partitioning $\mathcal{P}(\mathcal{X})$

$W \rightarrow \mathbf{0}_{n \times n}$

parallel do

for all $i, j \in A \subset \mathcal{P}(\mathcal{X})$ **do**

$k \leftarrow 1$

while $k \leq m$ **do**

$W[i, j] = W[i, j] + \phi^{n-k} \times \text{intersect}(S_{i,k}, S_{j,k})$

$k \leftarrow k + 1$

end while

end for

end parallel

C. Symmetric Non-negative Matrix Factorization

$D = \text{diag}(d_i)$ **where** $d_i = \sum_{j=1}^m W[i, j]$

$\hat{W} = D^{-\frac{1}{2}} W D^{\frac{1}{2}}$

$H^* = \min\{H \in \mathbb{R}_+^{n \times n_S} \mid \|W - HH^T\|^2\}$

for all $j \in \mathcal{X}$ **do**

$j^* = \{j \mid \max_{j \in \{1, \dots, n_S\}} H^*[i, j]\}$

$i \in A_{j^*}$

end for

Output: Set of clusters (A_1, \dots, A_{n_S})

C Linear model predictive control formulation

We report the non-linear and linear model of traffic dynamics as well as the MPC formulation used by [76] to render the paper self-contained.

Non-linear aggregated dynamics for a partitioned city

Consider an urban network partitioned into N homogeneous regions. For each region $i \in \mathcal{N} = \{1, \dots, N\}$ define:

- $n_i(k)$: total accumulation of region i ,
- $n_{ij}(k)$: vehicles in region i with destination region j ,
- $q_{ij}(k)$: exogenous demand generated in region i for destination j ,
- \mathcal{N}_i : set of adjacent regions to i ,
- $M_{ij}^h(k)$: transfer flow from region i to region h for vehicles destined to j ,
- $M_{ii}(k)$: internal trip completion rate of region i .

The sampling period is denoted by T_p . The state dynamics are modeled as

$$n_{ii}(k+1) = n_{ii}(k) + T_p \left(q_{ii}(k) - M_{ii}(k) - \sum_{h \in \mathcal{N}_i} M_{ii}^h(k) + \sum_{h \in \mathcal{N}_i} M_{hi}^i(k) \right), \quad (11)$$

$$n_{ij}(k+1) = n_{ij}(k) + T_p \left(q_{ij}(k) - \sum_{h \in \mathcal{N}_i} M_{ij}^h(k) + \sum_{h \in \mathcal{N}_i} M_{hj}^i(k) \right), \quad i \neq j. \quad (12)$$

The total accumulation in region i is

$$n_i(k) = \sum_{j \in \mathcal{N}} n_{ij}(k). \quad (13)$$

Each region has a production MFD $P_i(n_i(k))$ [veh · m/sec] between accumulation and total production. Let L_i be the average trip length and $\theta_{ij}^h(k)$ the routing proportions. The internal trip completion rate is defined as

$$M_{ii}(k) = \theta_{ii}(k) \frac{n_{ii}(k)}{n_i(k)} \frac{P_i(n_i(k))}{L_i}. \quad (14)$$

while the transfer flows are

$$M_{ij}^h(k) = \min \left\{ C_{ih}(n_h(k)), u_{ih}(k_c) \theta_{ij}^h(k) \frac{n_{ij}(k)}{n_i(k)} \frac{P_i(n_i(k))}{L_i} \right\}, \quad (15)$$

where $k_c = \lfloor k/N_c \rfloor$ is the control time index and $C_{ih}(n_h(k))$ is the receiving capacity. The control constraints are

$$0 \leq u_{ih}(k_c) \leq 1, \quad \forall i \in \mathcal{N}, h \in \mathcal{N}_i, \quad (16)$$

$$|u_{ih}(k_c) - u_{ih}(k_c - 1)| \leq u_{ih}^R. \quad (17)$$

A gridlock avoidance constraint ensures that

$$0 \leq n_i(k) \leq n_{i,\max}. \quad (18)$$

We can now formulate the non-linear MPC problem for prediction horizon N_p as

$$\max_{\{n_{ij}(k), u_{ih}(k_c)\}} \sum_{k=k_p}^{k_p+N_p-1} \sum_{i \in \mathcal{N}} L_i [M_{ii}(k) + u_{ih}(k_c) M_{ij}^h(k)] \quad (19)$$

$$\text{s.t. (11) - (18),} \quad (20)$$

$$k = k_p, k_p + 1, \dots, k_p + N_p - 1, \forall i, j \in \mathcal{N}, h \in \mathcal{N}_i \quad (21)$$

$$k_c = \left\lfloor \frac{k}{N_c} \right\rfloor, \quad (22)$$

Linearised model and linear MPC

Following the linearisation procedure in [76], three approximations are used:

1. Accumulation proportions $\alpha_{ij}(k) = n_{ij}(k)/n_i(k)$ are treated as exogenous constants over the horizon.
2. The MFD is approximated by piecewise-affine (PWA) functions $G_i(n_i) = G_i^\ell(n_i)$, $\ell = 1, \dots, N_i$.
3. Linear decision variables are introduced:

$$f_{ii}(k) = u_{ii}(k) G_i(n_i(k)) \theta_{ii}(k) \alpha_{ii}(k), \quad (23)$$

$$f_{ih}(k) = u_{ih}(k) G_i(n_i(k)) \sum_{j \in \mathcal{N}} \theta_{ij}^h(k) \alpha_{ij}(k). \quad (24)$$

The linear approximation of the state dynamics is written as

$$n_i(k+1) = n_i(k) + T_p \left(q_i(k) - f_{ii}(k) - \sum_{h \in \mathcal{N}_i} f_{ih}(k) + \sum_{h \in \mathcal{N}_i} f_{hi}(k) \right). \quad (25)$$

constrained to

$$0 \leq f_{ii}(k) \leq \theta_{ii}(k) \alpha_{ii}(k) G_i^\ell(n_i(k)), \quad (26)$$

$$0 \leq f_{ih}(k) \leq G_i^\ell(n_i(k)) \sum_{j \in \mathcal{N}} \theta_{ij}^h(k) \alpha_{ij}(k), \quad (27)$$

$$0 \leq n_i(k) \leq n_{i,\max}. \quad (28)$$

Optional linearised rate constraints:

$$f_{ih}(k_p) \leq \left(u_{ih}^{P,R} + u_{ih}^R \right) G_i^P(n_i(k_p)) \sum_j \theta_{ij}^h(k_p) \alpha_{ij}(k_p), \quad (29)$$

$$f_{ih}(k_p) \geq \left(u_{ih}^{P,R} - u_{ih}^R \right) G_i^P(n_i(k_p)) \sum_j \theta_{ij}^h(k_p) \alpha_{ij}(k_p). \quad (30)$$

The linear MPC objective is then

$$\max_{\{n_i(k), f_{ii}(k), f_{ih}(k)\}} \sum_{k=k_p}^{k_p+N_p-1} \sum_{i \in \mathcal{N}} L_i [f_{ii}(k) + f_{ih}(k)] \quad (31)$$

subject to the linear dynamics and constraints above. This is the controller used as comparison to DeePC in Section 4.

D Simulation and control parameters

In this section we detail the parameters used in Section 4 by the controllers and the simulation package

Lattice network

The seed used by SUMO is 42.

MPC: The prediction horizon has value $N_p = 4$; the number of piecewise components used in the piecewise linear approximation of the MFD is $N_i = 10$.

DeePC: The prediction horizon has value $T_f = 4$ and the past trajectory length is $T_{ini} = 5$. The parameters used in the cost function have value

$$\lambda_1 = 1, \lambda_2 = 1, \lambda_y = 0, Q = \begin{bmatrix} 1 & 0 \\ 0 & 1 \end{bmatrix}, \quad \begin{bmatrix} 2 & 0 \\ 0 & 2 \end{bmatrix}$$

Zürich network

The seed used by SUMO is 2389.

MPC: The prediction horizon has value $N_p = 4$; the number of piecewise components used in the piecewise linear approximation of the MFD is $N_i = 10$.

DeePC: The prediction horizon has value $T_f = 4$ and the past trajectory length is $T_{ini} = 5$. The parameters used in the cost function have value

$$\lambda_1 = 15, \lambda_2 = 20, \lambda_y = 0, Q = \begin{bmatrix} 1 & 0 & 0 & 0 & 0 & 0 & 0 & 0 \\ 0 & 1 & 0 & 0 & 0 & 0 & 0 & 0 \\ 0 & 0 & 1 & 0 & 0 & 0 & 0 & 0 \\ 0 & 0 & 0 & 1 & 0 & 0 & 0 & 0 \\ 0 & 0 & 0 & 0 & 1 & 0 & 0 & 0 \\ 0 & 0 & 0 & 0 & 0 & 1 & 0 & 0 \\ 0 & 0 & 0 & 0 & 0 & 0 & 1 & 0 \\ 0 & 0 & 0 & 0 & 0 & 0 & 0 & 1 \end{bmatrix}, \quad R = \begin{bmatrix} 2 & 0 & 0 & 0 & 0 & 0 & 0 & 0 \\ 0 & 2 & 0 & 0 & 0 & 0 & 0 & 0 \\ 0 & 0 & 2 & 0 & 0 & 0 & 0 & 0 \\ 0 & 0 & 0 & 2 & 0 & 0 & 0 & 0 \\ 0 & 0 & 0 & 0 & 2 & 0 & 0 & 0 \\ 0 & 0 & 0 & 0 & 0 & 2 & 0 & 0 \\ 0 & 0 & 0 & 0 & 0 & 0 & 2 & 0 \\ 0 & 0 & 0 & 0 & 0 & 0 & 0 & 2 \end{bmatrix}$$

References

- [1] United Nations. (2018) 68% of the world population projected to live in urban areas by 2050, says un. [Online]. Available: <https://www.un.org/development/desa/en/news/population/2018-revision-of-world-urbanization-prospects.html>
- [2] European Commission and Directorate-General for Mobility and Transport, *EU transport in figures – Statistical pocketbook 2022*. Publications Office of the European Union, 2022.
- [3] R. Diemer and F. Dittrich, *Transport in the European Union: current trends and issues*. Directorate-General for Mobility and Transport of the European Union, 2019.
- [4] P. J. Landrigan, “Air pollution and health,” *The Lancet Public Health*, vol. 2, no. 1, pp. e4–e5, Jan 2017. [Online]. Available: [https://doi.org/10.1016/S2468-2667\(16\)30023-8](https://doi.org/10.1016/S2468-2667(16)30023-8)
- [5] M. Raposo, I. Vandecasteele, and et al., “The future of road transport,” no. KJ-1A-29748-EN-N (online), KJ-1A-29748-EN-C (print), 2019.
- [6] D. Braess, A. Nagurney, and T. Wakolbinger, “On a paradox of traffic planning,” *Transportation Science*, vol. 39, no. 4, pp. 446–450, 2005. [Online]. Available: <https://homepage.rub.de/Dietrich.Braess/Paradox-BNW.pdf>

- [7] M. Papageorgiou, C. Diakaki, V. Dinopoulou, A. Kotsialos, and Y. Wang, “Review of road traffic control strategies,” *Proceedings of the IEEE*, vol. 91, no. 12, pp. 2043–2067, 2003.
- [8] N. Geroliminis, J. Haddad, and M. Ramezani, “Optimal perimeter control for two urban regions with macroscopic fundamental diagrams: A model predictive approach,” *IEEE Transactions on Intelligent Transportation Systems*, vol. 14, no. 1, pp. 348–359, 2013.
- [9] A. Kouvelas, M. Saeedmanesh, and N. Geroliminis, “A linear-parameter-varying formulation for model predictive perimeter control in multi-region mfd urban networks,” *Transportation Science*, vol. 57, no. 6, pp. 1496–1515, 2023. [Online]. Available: <https://doi.org/10.1287/trsc.2022.0103>
- [10] A. Rimoldi, C. Cenedese, A. Padoan, F. Dörfler, and J. Lygeros, “Urban traffic congestion control: A deepc change,” in *2024 European Control Conference (ECC)*. Piscataway, NJ: IEEE, 2024, Conference Paper, pp. 2909 – 2914, 22nd European Control Conference (ECC 2024); Conference Location: Stockholm, Sweden; Conference Date: June 25-28, 2024.
- [11] I. Arel, C. Liu, T. Urbanik, and A. Kohls, “Reinforcement learning-based multi-agent system for network traffic signal control,” *Intelligent Transport Systems, IET*, vol. 4, pp. 128 – 135, 07 2010.
- [12] B. Parasumanna Gokulan, X. German, and D. Srinivasan, “Urban traffic signal control using reinforcement learning agents,” *Intelligent Transport Systems, IET*, vol. 4, pp. 177 – 188, 10 2010.
- [13] A. L. C. Bazzan, “A distributed approach for coordination of traffic signal agents,” *Autonomous Agents and Multi-Agent Systems*, vol. 10, no. 1, pp. 131–164, Jan 2005. [Online]. Available: <https://doi.org/10.1007/s10458-004-6975-9>
- [14] F. V. Webster. (1958) Traffic signal settings. [Online]. Available: <https://trid.trb.org/view/113579>
- [15] D. Robertson, “Transyt method for area traffic control,” *Transportation Engineering & Control*, vol. 11, pp. 276–281, 1969.
- [16] M. Eom and B. Kim, “The traffic signal control problem for intersections: a review,” *European Transport Research Review*, vol. 12, no. 1, p. 50, Sep 2020. [Online]. Available: <https://doi.org/10.1186/s12544-020-00440-8>
- [17] S. S. S. M. Qadri, M. Gökçe, and E. Oner, “State-of-art review of traffic signal control methods: challenges and opportunities,” *European Transport Research Review*, vol. 12, pp. 1–23, 10 2020.
- [18] M. C. Dunne and R. B. Potts, “Algorithm for traffic control,” *Operations Research*, vol. 12, no. 6, pp. 870–881, 1964. [Online]. Available: <http://www.jstor.org/stable/168173>
- [19] P. G. Michalopoulos and G. Stephanopoulos, “Oversaturated signal systems with queue length constraints—i: Single intersection,” *Transportation Research*, vol. 11, no. 6, pp. 413–421, 1977. [Online]. Available: <https://www.sciencedirect.com/science/article/pii/0041164777900065>
- [20] —, “Oversaturated signal systems with queue length constraints—ii: Systems of intersections,” *Transportation Research*, vol. 11, no. 6, pp. 423–428, 1977. [Online]. Available: <https://www.sciencedirect.com/science/article/pii/0041164777900077>
- [21] L. Zadeh, “Fuzzy sets,” *Information and Control*, vol. 8, no. 3, pp. 338–353, 1965. [Online]. Available: <https://www.sciencedirect.com/science/article/pii/S001999586590241X>
- [22] S. Mohanaselvi and B. Shanpriya, “Application of fuzzy logic to control traffic signals,” *AIP Conference Proceedings*, vol. 2112, no. 1, p. 020045, 06 2019. [Online]. Available: <https://doi.org/10.1063/1.5112230>
- [23] S. Chiu and S. Chand, “Adaptive traffic signal control using fuzzy logic,” in *Proceedings. The First IEEE Regional Conference on Aerospace Control Systems,*, 1993, pp. 122–126.
- [24] C. P. Pappis and E. H. Mamdani, “A fuzzy logic controller for a trafic junction,” *IEEE Transactions on Systems, Man, and Cybernetics*, vol. 7, no. 10, pp. 707–717, 1977.

- [25] Y. S. Murat and E. Gedizlioglu, “A fuzzy logic multi-phased signal control model for isolated junctions,” *Transportation Research Part C: Emerging Technologies*, vol. 13, no. 1, pp. 19–36, 2005. [Online]. Available: <https://www.sciencedirect.com/science/article/pii/S0968090X04000683>
- [26] W. Ekeila, T. Sayed, and M. Elesaway, “Development of dynamic transit signal priority strategy,” *Transportation Research Record*, vol. 2111, pp. 1–9, 12 2009.
- [27] J. Niittymäki and M. Pursula, “Signal control using fuzzy logic,” *Fuzzy Sets and Systems*, vol. 116, no. 1, pp. 11–22, 2000. [Online]. Available: <https://www.sciencedirect.com/science/article/pii/S0165011499000342>
- [28] S. Sen and L. Head, “Controlled optimization of phases at an intersection,” *Transportation Science*, vol. 31, pp. 5–17, 02 1997.
- [29] P. Mirchandani and L. Head, “A real-time traffic signal control system: architecture, algorithms, and analysis,” *Transportation Research Part C: Emerging Technologies*, vol. 9, no. 6, pp. 415–432, 2001. [Online]. Available: <https://www.sciencedirect.com/science/article/pii/S0968090X00000474>
- [30] C. Cai, C. K. Wong, and B. G. Heydecker, “Adaptive traffic signal control using approximate dynamic programming,” *Transportation Research Part C: Emerging Technologies*, vol. 17, no. 5, pp. 456–474, 2009, artificial Intelligence in Transportation Analysis: Approaches, Methods, and Applications. [Online]. Available: <https://www.sciencedirect.com/science/article/pii/S0968090X09000321>
- [31] X. Zheng and W. Recker, “An adaptive control algorithm for traffic-actuated signals,” *Transportation Research Part C: Emerging Technologies*, vol. 30, pp. 93–115, 2013. [Online]. Available: <https://www.sciencedirect.com/science/article/pii/S0968090X13000375>
- [32] D. McKenney and T. White, “Distributed and adaptive traffic signal control within a realistic traffic simulation,” *Eng. Appl. Artif. Intell.*, vol. 26, pp. 574–583, 2013. [Online]. Available: <https://api.semanticscholar.org/CorpusID:36526311>
- [33] I. A. Villalobos, A. S. Poznyak, and A. M. Tamayo, “Urban traffic control problem: a game theory approach,” *IFAC Proceedings Volumes*, vol. 41, no. 2, pp. 7154–7159, 2008, 17th IFAC World Congress. [Online]. Available: <https://www.sciencedirect.com/science/article/pii/S1474667016400960>
- [34] M. C. Choy, D. Srinivasan, and R. Cheu, “Cooperative, hybrid agent architecture for real-time traffic signal control,” *IEEE Transactions on Systems, Man, and Cybernetics - Part A: Systems and Humans*, vol. 33, no. 5, pp. 597–607, 2003.
- [35] P. Varaiya, “Max pressure control of a network of signalized intersections,” *Transportation Research Part C: Emerging Technologies*, vol. 36, pp. 177–195, Nov. 2013. [Online]. Available: <https://www.sciencedirect.com/science/article/pii/S0968090X13001782>
- [36] T. Wongpiromsarn, T. Uthaicharoenpong, Y. Wang, E. Frazzoli, and D. Wang, “Distributed traffic signal control for maximum network throughput,” in *2012 15th International IEEE Conference on Intelligent Transportation Systems*, Sep. 2012, pp. 588–595, iSSN: 2153-0017. [Online]. Available: <https://ieeexplore.ieee.org/document/6338817>
- [37] L. Tassiulas and A. Ephremides, “Stability properties of constrained queueing systems and scheduling policies for maximum throughput in multihop radio networks,” *IEEE Transactions on Automatic Control*, vol. 37, no. 12, pp. 1936–1948, Dec. 1992. [Online]. Available: <https://ieeexplore.ieee.org/document/182479>
- [38] P. Scokaert, D. Mayne, and J. Rawlings, “Suboptimal model predictive control (feasibility implies stability),” *IEEE Transactions on Automatic Control*, vol. 44, no. 3, pp. 648–654, 1999.
- [39] N. Geroliminis and D. C. F., “Macroscopic modelling of traffic in cities,” *86th Annual Meeting Transportation Research Board*, vol. 42, 2007.

- [40] N. Geroliminis and C. F. Daganzo, “Existence of urban-scale macroscopic fundamental diagrams: Some experimental findings,” *Transportation Research Part B: Methodological*, vol. 42, no. 9, pp. 759–770, 2008. [Online]. Available: <https://www.sciencedirect.com/science/article/pii/S0191261508000180>
- [41] N. Geroliminis and J. Sun, “Properties of a well-defined macroscopic fundamental diagram for urban traffic,” *Transportation Research Part B: Methodological*, vol. 45, no. 3, pp. 605–617, 2011. [Online]. Available: <https://www.sciencedirect.com/science/article/pii/S0191261510001372>
- [42] I. I. Sirmatel and N. Geroliminis, “Economic model predictive control of large-scale urban road networks via perimeter control and regional route guidance,” *IEEE Transactions on Intelligent Transportation Systems*, vol. 19, no. 4, pp. 1112–1121, 2018.
- [43] S. Lin, B. De Schutter, Y. Xi, and H. Hellendoorn, “Efficient network-wide model-based predictive control for urban traffic networks,” *Transportation Research Part C: Emerging Technologies*, vol. 24, pp. 122–140, 2012. [Online]. Available: <https://www.sciencedirect.com/science/article/pii/S0968090X12000150>
- [44] I. Markovskiy and F. Dörfler, “Behavioral systems theory in data-driven analysis, signal processing, and control,” *Annual Reviews in Control*, vol. 52, pp. 42–64, 2021. [Online]. Available: <https://www.sciencedirect.com/science/article/pii/S1367578821000754>
- [45] J. C. Willems, “From time series to linear system—part i. finite dimensional linear time invariant systems,” *Automatica*, vol. 22, no. 5, pp. 561–580, 1986. [Online]. Available: <https://www.sciencedirect.com/science/article/pii/000510988690066X>
- [46] J. Coulson, J. Lygeros, and F. Dörfler, “Data-enabled predictive control: In the shallows of the deepc,” in *2019 18th European Control Conference (ECC)*, 2019, pp. 307–312.
- [47] P. G. Carlet, A. Favato, S. Bolognani, and F. Dörfler, “Data-driven predictive current control for synchronous motor drives,” in *2020 IEEE Energy Conversion Congress and Exposition (ECCE)*, 2020, pp. 5148–5154.
- [48] L. Huang, J. Coulson, J. Lygeros, and F. Dörfler, “Data-enabled predictive control for grid-connected power converters.” Piscataway, NJ: IEEE, 2019-12, Conference Paper, pp. 8130 – 8135, 58th IEEE Conference on Decision and Control (CDC 2019); Conference Location: Nice, France; Conference Date: December 11-13, 2019; Conference lecture held on December 13, 2019.
- [49] J. Wang, Y. Zheng, K. Li, and Q. Xu, “Deep-lcc: Data-enabled predictive leading cruise control in mixed traffic flow,” *IEEE Transactions on Control Systems Technology*, vol. 31, no. 6, pp. 2760–2776, 2023.
- [50] P. Zhu, G. Ferrari-Trecate, and N. Geroliminis, “Data-enabled predictive control for empty vehicle rebalancing,” in *2023 European Control Conference (ECC)*, 2023, pp. 1–6.
- [51] G. Deng, “Simulation-based optimization doctoral dissertation,” Ph.D. dissertation, University of Wisconsin-Madison, 2007.
- [52] Aimsun, *Aimsun Next 24 User’s Manual*, aimsun next 24.0.0 ed., Barcelona, Spain, Accessed on: Month, Day, Year 2024. [Online]. [Online]. Available: <https://docs.aimsun.com/next/24.0.0>
- [53] L. Owen, Y. Zhang, L. Rao, and G. McHale, “Street and traffic simulation: traffic flow simulation using corsim.” 01 2000, pp. 1143–1147.
- [54] A. Horni, K. Nagel, and K. Axhausen, *MATSim*. London: Ubiquity Press, 2016.
- [55] P. Kachroo and K. Ozbay, *Paramics*. Boston, MA: Springer US, 2003, pp. 293–327. [Online]. Available: https://doi.org/10.1007/978-1-4419-8961-1_12
- [56] P. A. Lopez, M. Behrisch, L. Bieker-Walz, J. Erdmann, Y.-P. Flötteröd, R. Hilbrich, L. Lücken, J. Rummel, P. Wagner, and E. Wießner, “Microscopic traffic simulation using sumo,” in *The 21st IEEE*

- International Conference on Intelligent Transportation Systems*. IEEE, 2018. [Online]. Available: <https://elib.dlr.de/124092/>
- [57] M. Fellendorf and P. Vortisch, *Microscopic traffic flow simulator VISSIM*, 06 2011, pp. 63–93.
- [58] S. Chen and D. J. Sun, “An improved adaptive signal control method for isolated signalized intersection based on dynamic programming,” *IEEE Intelligent Transportation Systems Magazine*, vol. 8, no. 4, pp. 4–14, 2016.
- [59] M. Miletić, B. Kapusta, and E. Ivanjko, “Comparison of two approaches for preemptive traffic light control,” in *2018 International Symposium ELMAR*, 2018, pp. 57–62.
- [60] D. Garg, M. Chli, and G. Vogiatzis, “Deep reinforcement learning for autonomous traffic light control,” in *2018 3rd IEEE International Conference on Intelligent Transportation Engineering (ICITE)*, 2018, pp. 214–218.
- [61] K. Jintamuttha, B. Watanapa, and N. Charoenkitkarn, “Dynamic traffic light timing optimization model using bat algorithm,” in *2016 2nd International Conference on Control Science and Systems Engineering (ICCSSE)*, 2016, pp. 181–185.
- [62] E. K. E. Ahmed, A. M. A. Khalifa, and A. Kheiri, “Evolutionary computation for static traffic light cycle optimisation,” in *2018 International Conference on Computer, Control, Electrical, and Electronics Engineering (ICCCEE)*, 2018, pp. 1–6.
- [63] S. Araghi, A. Khosravi, D. Creighton, and S. Nahavandi, “Influence of meta-heuristic optimization on the performance of adaptive interval type2-fuzzy traffic signal controllers,” *Expert Systems with Applications*, vol. 71, pp. 493–503, 2017. [Online]. Available: <https://www.sciencedirect.com/science/article/pii/S0957417416305966>
- [64] F. Ahmed and Y. Hawas, “An integrated real-time traffic signal system for transit signal priority, incident detection and congestion management,” *Transportation Research Part C: Emerging Technologies*, vol. 60, pp. 52–76, 2015. [Online]. Available: <https://www.sciencedirect.com/science/article/pii/S0968090X15002727>
- [65] A. Hajbabaie and R. F. Benekohal, “A program for simultaneous network signal timing optimization and traffic assignment,” *IEEE Transactions on Intelligent Transportation Systems*, vol. 16, no. 5, pp. 2573–2586, 2015.
- [66] S. Araghi, A. Khosravi, and D. Creighton, “Intelligent cuckoo search optimized traffic signal controllers for multi-intersection network,” *Expert Systems with Applications*, vol. 42, no. 9, pp. 4422–4431, 2015. [Online]. Available: <https://www.sciencedirect.com/science/article/pii/S095741741500086X>
- [67] Z. Li, M. Shahidehpour, S. Bahramirad, and A. Khodaei, “Optimizing traffic signal settings in smart cities,” *IEEE Transactions on Smart Grid*, vol. 8, no. 5, pp. 2382–2393, 2017.
- [68] S. S. Sultan Mohiuddin Qadri, M. Ali Gökçe, E. Öner, and E. G. Gökçe, “Analysis of various scenarios to mitigate congestion at a signalized roundabout using microsimulation,” in *2019 Innovations in Intelligent Systems and Applications Conference (ASYU)*, 2019, pp. 1–6.
- [69] M. A. Gökçe, E. Öner, and G. Işık, “Traffic signal optimization with particle swarm optimization for signalized roundabouts,” *SIMULATION*, vol. 91, no. 5, pp. 456–466, 2015. [Online]. Available: <https://doi.org/10.1177/0037549715581473>
- [70] S. Dabiri and M. Abbas, “Arterial traffic signal optimization using particle swarm optimization in an integrated vissim-matlab simulation environment,” in *2016 IEEE 19th International Conference on Intelligent Transportation Systems (ITSC)*, 2016, pp. 766–771.

- [71] I. Dakic, J. Stevanovic, and A. Stevanovic, "Backpressure traffic control algorithms in field-like signal operations," in *2015 IEEE 18th International Conference on Intelligent Transportation Systems*, 2015, pp. 137–142.
- [72] L. Zheng, X. Xue, C. Xu, and B. Ran, "A stochastic simulation-based optimization method for equitable and efficient network-wide signal timing under uncertainties," *Transportation Research Part B: Methodological*, vol. 122, pp. 287–308, 2019. [Online]. Available: <https://www.sciencedirect.com/science/article/pii/S019126151830403X>
- [73] D. Pavleski, D. Koltovska-Nechoska, and E. Ivanjko, "Evaluation of adaptive traffic control system utopia using microscopic simulation," in *2017 International Symposium ELMAR*, 2017, pp. 17–20.
- [74] P. T. M. Nguyen, B. N. Passow, and Y. Yang, "Improving anytime behavior for traffic signal control optimization based on nsga-ii and local search," in *2016 International Joint Conference on Neural Networks (IJCNN)*, 2016, pp. 4611–4618.
- [75] X. Chen, C. Osorio, and B. F. Santos, "Simulation-based travel time reliable signal control," *Transportation Science*, vol. 53, no. 2, pp. 523–544, 2019. [Online]. Available: <https://doi.org/10.1287/trsc.2017.0812>
- [76] A. Kouvelas, M. Saeedmanesh, and N. Geroliminis, "A linear formulation for model predictive perimeter traffic control in cities," *IFAC-PapersOnLine*, vol. 50, no. 1, pp. 8543–8548, 2017, 20th IFAC World Congress. [Online]. Available: <https://www.sciencedirect.com/science/article/pii/S2405896317319572>
- [77] J. C. Willems, "The behavioral approach to open and interconnected systems," *IEEE Control Systems Magazine*, vol. 27, no. 6, pp. 46–99, 2007.
- [78] A. E. Ezugwu, A. M. Ikotun, O. O. Oyelade, L. Abualigah, J. O. Agushaka, C. I. Eke, and A. A. Akinyelu, "A comprehensive survey of clustering algorithms: State-of-the-art machine learning applications, taxonomy, challenges, and future research prospects," *Engineering Applications of Artificial Intelligence*, vol. 110, p. 104743, 2022. [Online]. Available: <https://www.sciencedirect.com/science/article/pii/S095219762200046X>
- [79] M. Saeedmanesh and N. Geroliminis, "Clustering of heterogeneous networks with directional flows based on "snake" similarities," *Transportation Research Part B: Methodological*, vol. 91, pp. 250–269, 2016. [Online]. Available: <https://www.sciencedirect.com/science/article/pii/S0191261515302605>
- [80] Z. Jia, C. Chen, B. Coifman, and P. Varaiya, "The pems algorithms for accurate, real-time estimates of g-factors and speeds from single-loop detectors," in *ITSC 2001. 2001 IEEE Intelligent Transportation Systems. Proceedings (Cat. No.01TH8585)*, 2001, pp. 536–541.
- [81] J. C. Herrera and A. M. Bayen, "Incorporation of lagrangian measurements in freeway traffic state estimation," *Transportation Research Part B: Methodological*, vol. 44, no. 4, pp. 460–481, 2010. [Online]. Available: <https://www.sciencedirect.com/science/article/pii/S0191261509001222>
- [82] C. G. Claudel and A. M. Bayen, "Guaranteed bounds for traffic flow parameters estimation using mixed lagrangian-eulerian sensing," in *2008 46th Annual Allerton Conference on Communication, Control, and Computing*, 2008, pp. 636–645.
- [83] S. V. Kumar and L. Vanajakshi, "Short-term traffic flow prediction using seasonal ARIMA model with limited input data," *European Transport Research Review*, vol. 7, no. 3, p. 21, Jun. 2015. [Online]. Available: <https://doi.org/10.1007/s12544-015-0170-8>
- [84] L. R. Foulds, H. A. do Nascimento, I. C. Calixto, B. R. Hall, and H. Longo, "A fuzzy set-based approach to origin–destination matrix estimation in urban traffic networks with imprecise data," *European Journal of Operational Research*, vol. 231, no. 1, pp. 190–201, 2013.

- [85] L. E. Olmos, S. Çolak, S. Shafiei, M. Saberi, and M. C. González, “Macroscopic dynamics and the collapse of urban traffic,” *Proceedings of the National Academy of Sciences*, vol. 115, no. 50, pp. 12 654–12 661, 2018.
- [86] N. H. Gartner, J. D. C. Little, and H. Gabbay, “Optimization of traffic signal settings by mixed-integer linear programming: Part i: The network coordination problem,” *Transportation Science*, vol. 9, no. 4, pp. 321–343, 1975. [Online]. Available: <http://www.jstor.org/stable/25767802>
- [87] J. C. Willems, “From time series to linear system - part ii. exact modelling,” *Automatica*, vol. 22, pp. 675–694, 1986. [Online]. Available: <https://api.semanticscholar.org/CorpusID:7620875>
- [88] —, “From time series to linear system—part iii: Approximate modelling,” *Automatica*, vol. 23, no. 1, pp. 87–115, 1987. [Online]. Available: <https://www.sciencedirect.com/science/article/pii/0005109887901208>
- [89] M. Kontorinaki, A. Spiliopoulou, C. Roncoli, and M. Papageorgiou, “First-order traffic flow models incorporating capacity drop: Overview and real-data validation,” *Transportation Research Part B: Methodological*, vol. 106, pp. 52–75, 2017. [Online]. Available: <https://www.sciencedirect.com/science/article/pii/S0191261516302351>
- [90] C. Wagner, C. Hoffmann, R. Sollacher, J. Wagenhuber, and B. Schürmann, “Second-order continuum traffic flow model,” *Phys. Rev. E*, vol. 54, pp. 5073–5085, Nov 1996. [Online]. Available: <https://link.aps.org/doi/10.1103/PhysRevE.54.5073>
- [91] F. Dörfler, J. Coulson, and I. Markovskiy, “Bridging direct and indirect data-driven control formulations via regularizations and relaxations,” *IEEE Transactions on Automatic Control*, vol. 68, no. 2, pp. 883–897, 2023.
- [92] E. Spin-Off. (2024) Transcality. [Online]. Available: <https://transcality.com/>
- [93] L. Ambühl and K. Axhausen, “A case study of zurich’s two-layered perimeter control,” 2018, transportation Research Arena (TRA) ; Conference date: 01-04-2018.
- [94] Y. Tang, C. Cenedese, A. Rimoldi, F. Dörfler, J. Lygeros, and A. Padoan, “Split-as-a-pro: behavioral control via operator splitting and alternating projections,” in *2025 European Control Conference (ECC)*, 2025, pp. 1495–1501.
- [95] J. C. Willems, *Models for Dynamics*. Wiesbaden: Vieweg+Teubner Verlag, 1989, pp. 171–269. [Online]. Available: https://doi.org/10.1007/978-3-322-96657-5_5
- [96] J. C. Willems, P. Rapisarda, I. Markovskiy, and B. L. De Moor, “A note on persistency of excitation,” *Systems & Control Letters*, vol. 54, no. 4, pp. 325–329, 2005. [Online]. Available: <https://www.sciencedirect.com/science/article/pii/S0167691104001434>
- [97] I. Markovskiy and F. Dörfler, “Identifiability in the behavioral setting,” *IEEE Transactions on Automatic Control*, vol. 68, no. 3, pp. 1667–1677, 2023.
- [98] J. Berberich, J. Köhler, M. Müller, and F. Allgöwer, “Linear tracking mpc for nonlinear systems part ii: The data-driven case,” *IEEE Transactions on Automatic Control*, vol. 67, pp. 1–1, 09 2022.
- [99] A. Padoan, F. Dörfler, and J. Lygeros, “Data-driven representations of conical, convex, and affine behaviors,” in *2023 62nd IEEE Conference on Decision and Control (CDC)*. Singapore: IEEE, 2023, Conference Paper, pp. 596 – 601, 62nd IEEE Conference on Decision and Control (CDC 2023); Conference Location: Singapore; Conference Date: December 13-15, 2023.